## ABSTRACT

New wound dressing based on nanocomposite polyvinyl alcohol/hyaluronan/ silver nanoparticles (PVA/HA/Ag-NPs) was prepared by *green way*. Hyaluronan was used as reducing and stabilizing agent for hyaluronan for silver nanoparticle preparation. Different parameters were investigated for preparation of Ag-NPs like concentration of silver nitrate as a source of Ag-NPs (0.01, 0.1, 0.5, 1M), concentration of HA (1, 2 %) and molecular weight of HA (50 kDA, 1,7 MDa). The nanofibers dressing sheet were fabricated by electro-spinning technique using different ratios between PVA and HA/Ag-NPs (100; 90/10; 80/20; 64/40; 50/50). The nanocomposites were evaluated by TEM, rheology, DLS, UV/Vis spectroscope, and the wound dressing nanofibers were characterized by SEM, TGA, FTIR, XRD and the mechanical properties were measured and evaluated.



## KEYWORDS

Nanocomposite, hyaluronan, silver nanoparticles, electrospinning, wound dressings



## ABSTRAKT

Boli pripravené kryty rán na bázi prírodných látok polyvinyl alcohol/ hyaluronan/ strieborné nanočastice (PVA/ HA/ Ag-NPs). Hyaluronan bol použitý ako redukčné a stabilizačné činidlo pre syntézu nanočastíc striebra. Pri príprave Ag-NPs boli testované viaceré parametre ako koncentrácia dusičnanu strieborného ako zdroja Ag-NPs (0,01; 0,1;0,5;1 M), koncentrácia kyseliny hyalurónovej (1,2 %) a jej rozdielna molekulová hmotnosť. Kryty rán z nanovlákien boli pripravené pomocou techniky electro-spinning z roztokov líšiacich sa pomerom PVA a HA/Ag-NPs (100; 90/10; 80/20; 60/40; 50/50). Vlastnosti nanokompozitu HA/Ag-NPs boli hodnotené pomocou TEM, reológie, DLS, XRD, UV/Vis spektroskopie a kryty rán boli charakterizované pomocou SEM, TGA, FTIR a ťahovej skúšky.



## KĽÚČOVÉ SLOVÁ

Nanokompozit, hyaluronan, strieborné nanočastice, electrospinning, kryty rán



ČILEKOVÁ, M. Kryty ran připravené z nanokompozitního materiálu. Brno: Vysoké učení technické v Brně, Fakulta chemická, 2018. 67 s. Vedoucí diplomové práce Dr. Abdelmohsan Abdellatif, Ph.D..

## DECLARATION

I declare that the diploma thesis has been worked out by myself and that all the quotations from the used literary sources are accurate and complete. The content of the diploma thesis is the property of the Faculty of Chemistry of Brno University of Technology and all commercial uses are allowed only if approved by both the supervisor and the dean of the Faculty of Chemistry, BUT.

.....
student's signature


## ACKNOWLEDGEMENT

I would like to thank to my supervisor Dr. Abdelmohsan Abdellatif, Ph.D. for his professional guidance, precious advices, positive attitude and willingness to help me anytime I needed. Furthermore, I would like to thank to Mgr. David Pavliňák, Ph.D., for introducing me to the topic of electrospinning and his guidance through all the process of the wound dressings preparation. With a special mention to Ing. Petr Lepcio I would like to express my gratitude not only for introducing me to the measurements, time helping me in the lab and final corrections but also for his overall support. Last but not least I must express my very profound gratitude to my loved ones, for all their love and support. Special thanks belongs to my mum for everything what she helped me to be. Thank you.

# CONTENT

# 1. THEORETICAL PART

## 1.1 Introduction

A wound is defined as a disruption in the continuity of the epithelial lining of the skin or mucosa resulting from physical or thermal damage. There are two types of wounds according to duration and nature of healing process, the wound is categorized as acute and chronic [1]. An acute wound is an injury to the skin that occurs suddenly due to accident. It heals at a predictable and expected time frame usually within 8-12 weeks depending on the size, depth and the extent of damage. Chronic wounds on the other hand fail to progress through the normal stages of healing and cannot be repaired in an orderly and timely manner. Chronic wounds generally result from decubitis ulcer, leg ulcer and burns.

Wound healing is a dynamic and complex process of tissue regeneration and growth progress through four phases (i) the coagulation and hemostasis phase (immediately after injury); (ii) the inflammatory phase, (shortly after injury to tissue) during which swelling takes place; (iii) the proliferation period, where new tissues and blood vessels are formed and (iv) the maturation phase, in which remodeling of new tissues takes place [2,3]. Promotion of these phases depends on wound type, pathological conditions and type of dressing material. There are more factors affecting healing ability of wounds as interactions among cytokines, growth factors, blood and the extracellular matrix. The cytokines promote healing by various pathways such as stimulating the production of components of the basement membrane, preventing dehydration, increasing inflammation of tissues. Local factors which includes hypothermia, pain, infection, radiation and tissue oxygen tension. In addition, age and nutrition also take place in healing ability of wounds. Some syndromes such as Ehlers-Danlos syndrome and Cutis Laxa are associated with abnormal healing that prolongs time of healing [1].

## 1.2 Wound dressings

With the advancement in technology, different types of wound dressing materials are available for all types of wounds. Selection of a material for a particular wound is important to achieve faster healing. There are criteria for choosing the right type of wound dressing. Wound dressing should have ability to provide or maintain moist environment, enhance epidermal migration, promote angiogenesis and connective tissue synthesis, allow gas exchange between wounded tissue and environment, maintain appropriate tissue temperature to improve the blood flow to the wound bed and enhances epidermal migration. It should also provide protection against bacterial infection, should be non-adherent to the wound and easy to remove after healing, must provide debridement action to enhance leucocytes migration and support the accumulation of enzyme and must be sterile, non-toxic and non-allergic [1].

### 1.2.1 History of wound care

It is important to care for wound properly and application of a wound dressing is part of this process. Wound dressing is designed to be in contact with wound that differs from bandage that just holds dressing in place. Historically, wet-to-dry dressing have been used. Mesopotamians used to clean wounds with water or honey prior to use of the honey or resin dressing from around 2500 BC. In 1600 BC, linen strips soaked in oil covered with plasters were used to cure

wounds. Ancient Greeks in 460-370 BC started to use wine or vinegar for cleaning wounds and honey, oil and wine as a further treatment. They used wool boiled in water or wine as a bandage [4].

### 1.2.2 Traditional wound care materials

Products including gauze, lint, plasters, bandages and cotton wool are dry and used for protecting wound from contamination. These dressings can be used as primary dressings right in contact with wound, or secondary dressings just to keep primary dressings in place. They protect wound against bacterial infection and some sterile gauze pads also absorb exudates and fluid from open wound. These dressings require frequent changing to protect from maceration healthy tissues. Due to excessive wound drainage it can become adherent to wound surface and cause painful removing of dressing. Generally, traditional dressings are suitable for clean and dry wounds with mild exudate, or as secondary dressing. Due to number of weak properties traditional dressings were replaced with modern dressing of advanced design which solved multiple application-related issues [4].

#### *1.2.2.1 Gauze*

Term gauze refers to two different bandage materials. It could mean either woven gauze, which is the 100 % natural cotton cloth that we are most familiar with or non-woven gauze, more modern, synthetic dressings made of rayon or synthetic fiber blends. Woven gauze is problematic in dressing as it sheds fibers when cut and may leave debris in the wound when removed, it also tends to stick to the wound.

Till 1962 it was believed that the best for healing wounds is dry environment. In winter 1962 research on pig model proved that moist wounds healed faster than dry wounds. Today, woven gauze can be often seen as ‘wet to dry’ dressing used in range of wound care strategies. It is also utilized as a carrier for antimicrobial agents. Gauze was also part of the first non-adherent dressing. First part was cotton mesh containing paraffin and a balsam for contact with the wound, while second comprised gauze which enabled drainage. Despite its drawbacks, it is still the most utilized wound dressing in the world. Factors such as cost, education and the ability to follow best practice determine usage of gauze even when technologic progress offer us many better alternatives [5].

### 1.2.3 Modern wound care materials

Modern wound dressings facilitate healing rather than just a simple cover. There was a major breakthrough in the antiseptic technique during the 19$^{th}$ century, antibiotics were introduced to control infections and decrease mortality. Modern wound dressing arrived in 20$^{th}$ century [5].

#### *1.2.3.1 Semi-permeable films*

Current semi-permeable films allow gas and water exchange while preventing bacterial migration into the wound. It could be non-porous, plasticized polyvinyl polymer films coupled with cotton-lint pads in first aid [6].

#### *1.2.3.2 Calcium or calcium/sodium alginate*

Calcium alginate is comprised of a natural polymer extracted from brown seaweed. It is dried and formed to a hard mass. Alginates are applied dry and are soaked from excess of moist from wound that makes gel from alginate fibers, prevent of maceration of surrounding healthy tissues. In the case that the moist from wound is insufficient to gel the fibers, dressings can leave residual debris as they are fibrous in structure [7].

#### *1.2.3.3 Spray-on dressings*

Nobecutan is a spray-on formulation of acrylic resin dissolved in a mixture of acetic esters. It forms a thin plastic film while organic solvent evaporates. In research, Nobecutan was found difficult to maintain a seal between the film and skin as a result of bleeding. In another hand spray-on dressings were useful in reducing rates in facial scrotal, and abdominal surgeries where application of traditional dressings was difficult. Currently, spray- on dressings are commercially available as a first aid for superficial acute wounds [8].

#### *1.2.3.4 Hydrocolloids*

Inner layer of hydrocolloid dressings is made from gelatin, pectin, sodium carboxymethylcellulose and polyisobutylene. Outer layer is film that is forming flexible wafer dressing. It provides moist, hypoxic wound environment that promotes autolytic debridement and allow gas change [6].

#### *1.2.3.5 Hydrogels*

Hydrogels consists of cross-linked polymers such as starch, cellulose and other plant or animal derived polysaccharides. They can provide moisture to dry wounds as they contain up to 96% water. They can also absorb excess exudate from wound. Hydrogels promote autolysis of necrotic tissue and don´t support bacterial growth.

Limitation of hydrogels are in usage for high exudate wounds, where there is the risk of maceration of surrounding healthy tissues and shifting from dry to wet gangrene in case of exuding ischematic ulcers. Hydrogels based on polyvinylpyrrolidone/polyethylene glycol reports some antimicrobial and antifungal properties. Hydrogels are used for treatment of burns, chronic ulcers, surgical wounds and even injected into spinal column [6].

#### *1.2.3.6 Foams*

Poyurethane foam dressings are easy to customize as they come in the range of absorbance and can be cut to required shape. They absorb excess wound exudate, maintain moist wound interface and provide thermal insulation. It also facilitate the removal of slough. There is wide range of foam dressings that incorporate other components to enhance absorbance, control infection or help ensure atraumatic removal. These foams can be used in both acute and chronic wounds [1].

#### *1.2.3.7 Silicone dressings*

Silicone is used as a contact dressing or as the contact layer within dressing. There is Mepilex, a polyurethane foam membrane coated with a soft silicon layer. Silicon is also used as coating

on materials like non-woven polyester nets. Silicone dressings are safe in atraumatic removal of dressings and can be used both for acute and chronic wounds [9].

#### *1.2.3.8 Capillary action dressing*

They consist of an absorbent pad made of hydrophilic fibers, typically 80% of polyester, 20% of cotton fibers. Absorbent pad is between two layers of perforated, permeable, non-woven polyester. Exudate is removed from the wound by capillary action. It decreases bacterial load on wound surface and helps with debridement and desloughing, but it may adhere to the wound. Optimal application involves conjunction with a non-adherent contact layer [10].

#### *1.2.3.9 Odor-absorbent dressing*

Odor in a wound is primarily produced from anaerobic bacteria. These dressings are made from charcoal or activated carbone which is shown to retain odor-causing molecules.

#### *1.2.3.10 Scaffolds*

Scaffolds are 3D supports that have rigid structure of nano and micro topography. Scaffolds facilitate infiltration of cells such as fibroblasts and keratinocytes through pores of controllable and maintain ideal healing conditions. Ideally, a dermal scaffold should mimic tissue's extracellular matrix (ECM) while allowing incorporation of bioactive molecules. Scaffolds can be either acellular or seeded with dermal cells. Acellular scaffolds made by decellularization of porcine or human tissue, what destroys cells which are subsequently washed off, leaving just ECM [11].

Dermal cells in the scaffolds promote healing through the secretion of growth factors and structural proteins. An example of a natural scaffold is chitosan and collagen. Chitosan is biopolymer derived from chitin, polymer found in abundant animal exoskeletons. Due to biocompatibility, degradability and low antigenicity is optimal material for scaffolds. The most used synthetic substance for scaffolds are based on lactic and glycolic acid. Synthetic polymers enable a range of strategies and new techniques in preparation of scaffolds. One of it is for instance electrospinning [12].

### 1.2.4 Antibacterial dressings

#### *1.2.4.1 Honey dressings*

Honey is antibacterial and antifungal against approximately 70 bacterial stains and some yeast. Antimicrobial action is mechanical and enzymatic. These dressings provide antimicrobial and anti-inflammatory properties through autolytic debriedement, it can inhibit bacterial growth due to osmolarity, when high concentration of sugars causes water to be drawn from the local wound environment. This also maintains a moist environment. Use of honey as an antibacterial is well established in modern wound care and is used in variety of modern wound dressings. Honey is applied like an ointment or it is impregnated on hydrogel or alginate dressings. As an ointment it dilutes rapidly due to wound exudate and increases fluidity due to body temperature, treatment then requires more often changes of dressings [6].

#### *1.2.4.2 Iodine dressings*

Iodine is natural antiseptic agent available in a range of topic applications. It targets broad spectrum of bacteria, fungi, viruses and prions. Iodophors were developed by complexing elemental iodine to a surfactant to improve solubility and reduce cytotoxicity effect of elemental iodine. The most utilized are povidone-iodine and cadexomer-iodine [6].

#### *1.2.4.3 Silver dressings*

Silver ions disrupt protein and nucleic acids of bacteria through interaction with their negatively charged groups as thiols, carboxylates, phosphates, hydroxyls, imidazoles, indoles and amines and it results in loss of viability. Although the antibacterial action of silver is well established, potential cytotoxicity remains an issue [1,6].

#### *1.2.4.4 Nanoparticles wound dressings*

Nanoparticles offer promising alternative to antibiotics, they have bactericidal activity against many strains and they reduce number of side effects of drugs and do not trigger microbial resistance. NPs can affect bacteria right by the contact with cell wall by releasing toxic metal ions when positively charged metal ions are attracted by negatively charged groups at the bacterial surface. Then physical bonds are created and cell wall permeability is altered through creation of pores what leads to destruction of microorganism. NPs can also cross cell wall and affect metabolic pathways, interact with DNA and lysosomes.

Among NPs the most attention gained silver NPs with inhibitory activity towards nearly 650 microbe species. Acticoat®, Aquacel Ag® and Silvasorb® are brands of products already using Ag NPs in wound dressing application [6]. In 2013 antibacterial properties of silver-nanoparticles/bacterial cellulose composites were confirmed where control sample of BC did not show any antibacterial properties, thus, this property had to be provided by silver NPs [13]. In the study of Austine, et al. good antibacterial properties of silver NPs against *S. aureus* and *E. coli* [14] were shown. The current trend is to combine nanoparticles with other natural products such as chitosan to increase biocompatibility [12].

According to polymer NPs nanocomposite interaction between filler and polymer enables the NPs to act as molecular bridges which greatly affects properties of the matrix. Bio polymers furthermore add bioactivity, biocompatibility and/or resorb-ability to the bio-nanocomposites [15].

### 1.2.5 Wound dressing based on hyaluronic acid

Study of Anisha, et al. worked with the Chitosan-HA/Ag NPs nanocomposite which showed that higher concentrations of Ag-NPs (0.005%, 0.01%, 0.2 %) had the greatest antibacterial effects against the most resistant gram positive microorganisms [16].

## 1.3 Nanocomposites

We know the three basic types of materials around us, these are polymers, metals and ceramics. By combination of two different chemical materials we obtain composite material. There are many examples of composite materials in the nature like wood which is combination of cellulose fiber and lignin binder as well as manmade tools as tennis rocket where graphite fibers

provide strength while epoxy polymer provides flexibility and bonding strength between graphite fibers. Nanocomposite is material in which at least one component has one or more dimension in nanometer range [17]. There is dependence of specific surface area of particles on their diameter.

Nanotechnology is rapidly growing field of study with equally fast rate of newly emerging applications [19]. The result of adding nanoparticles to the matrix is the improvement of many properties including mechanical strength, modulus, toughness, dimensional stability, electrical and thermal conductivity, flame retardancy, chemical resistance, or thermal stability. Effectiveness of added nanoparticles is very high so amount of added material is normally only 0,5-5 %. Nanoparticles have very high surface to volume ratio which promotes surface effects that dramatically change properties of nanocomposites compared to bulk material properties of the respective components [20]. In order to take advantage of this effect, dispersion of particles plays important role [21].

Nanocomposites are used in many applications such as in automotive and aerospace industry for producing tough and strong materials light at the same time, thin-films capacitors for computer chips, batteries with greater power output, flexible batteries, tumors markers or scaffolds which speeding up healing process of bones [22].

### 1.3.1 Polymer based nanocomposites

Polymer based nanomaterials are by far the most widely commercially used nanocomposites. Currently, the most used are carbon-filled, i.e. carbon black, carbon nanotubes, graphene, fullerene. Mainly in automotive, combination of polymer and clay nanoparticles is used what reduced 60 % of the weight of the parts like bumpers or roof-box covers and increase their resistant to scratching. Clay can significantly reduce gas/vapor permeation in beverage bottles and food packaging, where it is also used. CNTs offer excellent mechanical properties required from sport and electronic to automotive and military [19].

## 1.4 Hyaluronic acid

Hyaluronic acid is a high molecular polysaccharide consisting of basic disaccharide repeat, Glucuronic acid and N-acetyl glucosamine, connected with beta-1,3-glycoside bond. Hyaluronic acid (HA) is present in high concentration in extracellular spaces, promotes cell migration in embryogenesis [23].

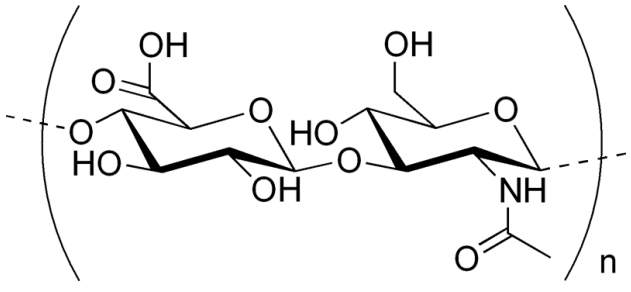


**Pic. 1:** Chemical formula of hyaluronic acid.

Repeatable disaccharide residue was established to has molecular mass of 397 Da. It also belongs to the class of mucopolysaccharides currently known as glycosaminoglycans. Mucopolysaccharides give viscous lubricating properties which are related to their ability to bind a significant amount of water. Hyaluronic acid was discovered in 1934 as extremely high molecular weight polysaccharide isolated from the vitreous of bovine eyes. Till now HA was isolated from various animal organs. It was found in joint fluid, the umbilical cord, cock´s combs and nowadays it is possible to extract HA from almost all vertebrate tissues. In 1937 was hyaluronan extracted even from the capsules of *streptococci* groups A and C, which is nowadays the most economical and reliable source for industrial production of hyaluronic acid.

Hyaluronan is synthetized by hyaluronan synthase connected with cytoplasmic cell membrane and it is removed through membrane directly on the outer cell surface to the extracellular matrix. In further research it was found that viscosity of HA solution in water could be related to pH and solution ionic strength. Different viscosities were observed in presence of the different inorganic salts. The highest viscosity was observed in solution of HA dissolved in distilled water.

It found medical applications mostly in eye surgery, treatment of joints diseases and aesthetic surgery. First real use of hyaluronic acid is dated to 1943 when during the Second World War bandages based on hyaluronic acid were used. The main component was extract from the umbilical cord. Method was later approved by USSR Ministry of Health and drug received name 'Regenerator'. In the second half of the 20th century new applications of HA were discovered in eye surgery, first injections to joints to treat arthritis in racehorses, treating wounds in order to prevent postoperative soldering, Since HA was used in implanted intraocular lenses, hyaluronan become one of the most important components in ophthalmology [24].

There is wide range of hyaluronic acid applications in practical medical applications nowadays. It has anti-inflammatory, disinfectant and wound healing effects. HA promotes epithelial regeneration, prevent from tissue granulation and protect internal eye tissues. HA also maintain normal water balance, skin hydration, moisture retention and improves elasticity and rate of skin regeneration. Its properties depend on molecular weight of the HA fraction as well. Moreover, it is environmentally friendly chemical used also as diagnostic marker for different diseases such as cancer [15].

There are different functions of hyaluronic acid dependent on its molecular weight. Fraction with molecular weight till 30 000 Da penetrate trans epidermal barrier, stimulate growth of the blood and lymphatic capillaries, improves microcirculation and nourishment of the skin. Fraction from 50 000 Da to 100 000 Da has wound healing properties, stimulate proliferation of cells and their migration into the wound. 500 000 Da – 730 000 Da HA suppress proliferation and migration of cells, inhibit growth of blood and lymphatic capillaries, prevent cartilage breakdown and reduce inflammatory processes. Critical role of MW HA/Ag-NPs and high MW HA without Ag-NPs to improve granulation and inflammatory mediators in impaired older and diabetic rat´s wound compared to other controlled samples of medium MW HA and low MW HA [25].

In the last years, study of HA was focused on new, very promising area: the targeted delivery of drugs to specific organs or tissues. Development of nanotechnology have brought new possibilities, as nanosized particles have a good ability to target delivery of biologically active compounds to the specific cell in the body. HA macromolecules could bind to the receptors of cytoplasmic membranes of various cell and target delivery of biologically active compounds attached to the biopolymer [24].

## 1.5 Electrospinning

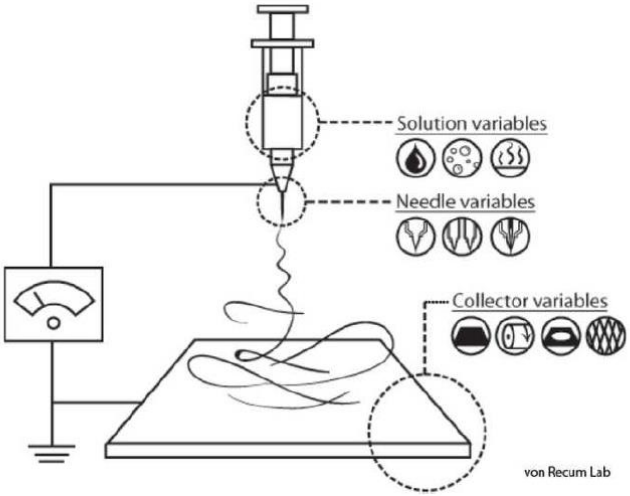


**Pic. 2:** Electrospinning from the tip of the syringe [26].

Nanofibers are nanostructures with diameter in scale of nanometers and longitudinal dimension much longer than the diameter. It is not exactly defined where is boundary of nanofibers. In some sources it is defined as fibers with diameter lower than 1 μm, other sources say diameter lower than 100 nm. The most widely prepared nanofibers are polymeric, but it is also possible to prepare nanofibers from metal, ceramics and carbon. For laboratory application, several techniques can be utilized for preparing nanofibers. There is for instance a technique based on pulling fibers from droplets suitable for further research of nanofibers, another one is pressing solution through the nano-sized diameter nozzles. Melt blowing is very productive for nanofibers production and can be modified to blow different fibers to the same required position, both microfibers and nanofibers what produces layers of fiber composite with smart material properties. Another effective method for nanofiber preparation is electrospinning [27].

From 1934 to 1944 was Antony Formhals from USA given first patents for electrospinning. In 1952 Neubauer and Vonnegut invented electrospraying, their machine prepared droplets with size approximately 0,1 mm. In 1966 Simon received patent for machine for electrostatic spinning, which prepared nonwoven fabrics. Simon observed the fact, the less viscous is solution for preparing nanofibers, the finest fibers with smaller diameter are prepared [28].

### 1.5.1 Principle of method

Electrospinning method uses high voltage electric field to form solid nanofibers from a polymeric solution or melt delivered conventionally through a millimeter-scale nozzle, see Pic. 2. Electrode can be either inserted in the polymer fluid, or it can be placed onto the tip of

the syringe. Mutual charge repulsion caused by electric field causes force directly opposite to the surface tension of the solution. As intensity of electric field is increased, hemispherical surface of the fluid starts to form Taylor cone. Due to overcoming surface tension by electrostatic force, jet of fluid ejected to the opposite electrode where nanofibers are collected usually at the top of the fabric.

Typically is electrospinning applicable to wide range of polymers as polyolefine, polyamides, polyesters, aramide as well as biopolymers like proteins, DNA, polypeptides or others. Collector is usually metal sheet covered with fiber. Advanced electrospinning can be provided at vacuum because higher electric field strength over large distances [29].

### 1.5.2 Conditions critical for electrospinning

Morphology and diameter of nanofibers depends on many parameters. These could be divided to parameters of polymer, parameters of solution and other parameters like intensity of electric field, geometry of used electrodes, ambient temperature and moisture.

Concentration, viscosity and electric conductivity of solution plays important role in electrospinning. At lower viscosities dominates influence of surface tension over electrostatic force and instead of fibers, droplets are produced, what refers to technique of electrospraying. According to studies, diameter of fibers is increasing with increasing concentration of solution and fiber diameter is decreased by increased electrical conductivity of the solution. By increased electric field is increased flow of the nanofibers as it is for polymer easier to produce Taylor cone, but at higher intensities of electric field are produces nanofibers with more defects. Distance between electrodes is important as with longer distance is longer the pathway of fiber formation, hence thinner fibers are possible to obtain, in another hand intensity of electric field is decreasing with longer distance between electrodes.

From ambient conditions are the most critical temperature and air moisture. These parameters influence speed of the solvent evaporation.

### 1.5.3 Nanospider™ by Elmarco

Nanospider™ is modified technique of electrospinning developed by Czech scientists in 2003, and it´s scheme could be seen in Pic. 3. Nanospider™ electrospinning technology from Elmarco is needle-free high voltage, free liquid surface electrospinning machine creating Taylor Cones and subsequent flow of material from a thin film of a polymer solution instead of tip of a capillary, generating many Taylor cones instead of one what increase efficiency of process. Technology uses two electrodes, cathode is rotating string electrode partially immersed in the polymer solution and anode is right behind [28].

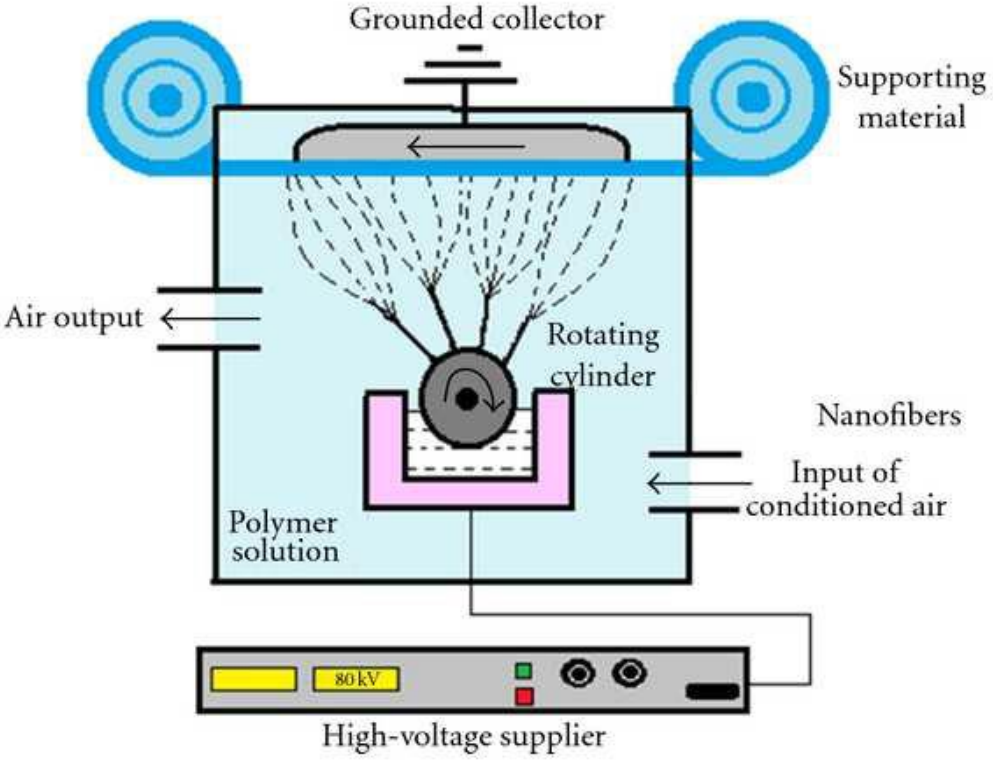


**Pic. 3**: Scheme of needle-free electrospinning [26].

# 2. EXPERIMENTAL PART

## 2.1 Materials

Sodium hyaluronate with molecular weight of 1.5-1.7 MDa was purchased from CPN Ltd., (Czech Republic), sodium hydroxide was purchased from Lach-Ner (Czech Republic) and silver nitrate was obtained from Sigma-Aldrich (Germany). 16 % PVA for electrospinning was kindly provided by department of physical electronics of Masaryk University in Brno. Milli-Q water was used for all the experiments.

## 2.2 Methods

### 2.2.1 Preparation of silver/hyaluronan nanoparticles nanocomposite

For preparation of 25 ml of HA/Ag-NPs nanocomposite was used further described process. 1% or 2 % HA solution was prepared by dissolving of corresponding weight of HA powder (stirring, 90 °C) in 23 ml of demineralized water into homogenous, viscous solution. Then, the pH was increased close to pH = 12 by 1 ml of NaOH (2 M) which was added drop-wise into hyaluronan solution under stirring condition at 90 °C providing basic hydrolysis of hyaluronic acid. Silver hyaluronate solution (1 ml) was added drop-wise into the hydrolyzed solution of hyaluronic acid and further reaction was running under stirring at 90 °C for 10, 20, 40 or 60 minutes and then cooled down to room temperature.

### 2.2.2 Preparation of nanocomposite wound dressing

HA/Ag-NPs nanocomposite solution was blended in ratios 50:50, 40:60, 20:80, 10:90, 5:95 with PVA. Nanofiber preparation was provided by Nanospider™ Elmarco (NSLAB 500 Czech Republic) at department of physical electronics of Masaryk University in Brno. Electrospinning was carried out at laboratory pressure and temperature. Rotating string electrode was used and distance between electrodes was fixed to 130 mm. Voltage of 58 kV was used and electrode was spinning at frequency approximately 24 Hz. Actual current was just observed as sign of well proceed electrospinning process. Nanofiber layer was continuously applied on the nonwoven fabric for approximately 30 minutes.

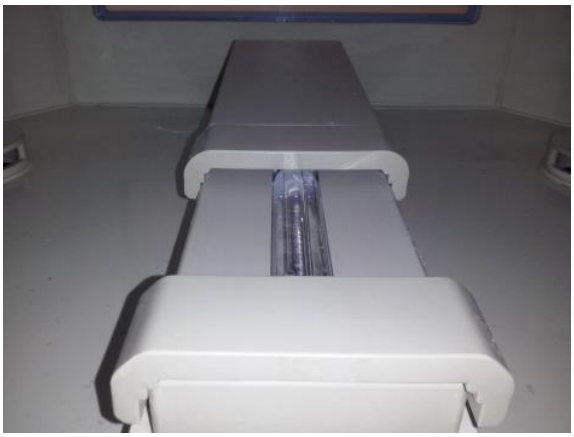

**Pic. 4**: Rotating string electrode in Nanospider NSLAB 500 Elmarco.


**Pic. 5:** Nanospider NSLAB 500 Elmarco.

## 2.3 Characterization of solution

### 2.3.1 UV-Vis spectroscopy (UV-Vis)

UV-Vis spectroscopy or UV-Vis spectrophotometry is absorption or reflectance spectroscopy technique in the ultraviolet-visible spectral region. Regarding to the laboratory equipment of today, UV-Vis uses radiation from 200 to 1000 nm and therefore partly includes the near infrared area (NIR) [30]. In visible spectral region is interaction between electromagnetic radiation and matter manifested as color and absorption or reflectance in the visible range directly affects perception of color. In this region of the electromagnetic spectrum, molecules undergo electronic transitions and by UV-Vis spectroscopy are measured transitions from the ground state to excited state. Practically, in this technique is measured attenuation of a beam of light after it passes through a sample or after reflection from sample surface. UV-Vis spectroscopy is a universal analytical and characterization technique. Linear relationship between absorbance and absorber concentration makes from UV-Vis reliable technique for quantitative measurements [31]. Qualitative measurement is provided due to different chemical structures absorb at different wavelength.

In this experiment was UV/Vis spectroscopy used to confirm synthesis of Ag NPs and absorption mode was carried out. Quartz cuvette was used for all measurements. Due to high value of absorbance of prepared samples, all of them were 10 times diluted. According to literature, silver absorbs UV/Vis at around 420 nm dependent also on size of nanoparticles [32].

### 2.3.2 Dynamic light scattering (DLS)

Dynamic light scattering also known as quasi-elastic light scattering or photon correlation spectroscopy is technique which analyzes diffusion coefficient and further calculate hydrodynamic radii by measuring the intensity of laser light scattered by molecules in solution. When monochromatic beam of light goes through solution with macromolecules, reflection of light depends on the size and shape of macromolecules [33]. While in static light scattering technique scattered light is analyzed as time averaged intensity and provides information about molecular weight and radius of gyration, DLS analyze intensity fluctuations of scattered light, hence provides information about diffusion coefficient and particle size. Intensity fluctuations are caused by constant moving of particles due to Brownian motion. DLS measures primarily Brownian motion of particles in solution relates this motion to the size of particle. Motion of macromolecules depends not only on their size, but also on temperature and viscosity. Large particles diffuse slowly, keeping the same or similar position at different time points, smaller particles (like molecules of solvent) move faster and adopt different positions at time [34]. As bigger particles move slower, they also response with slower time intensity fluctuations of light while quickly moving small particles have fast intensity fluctuations of light as it is visible from scheme in Pic. 6.

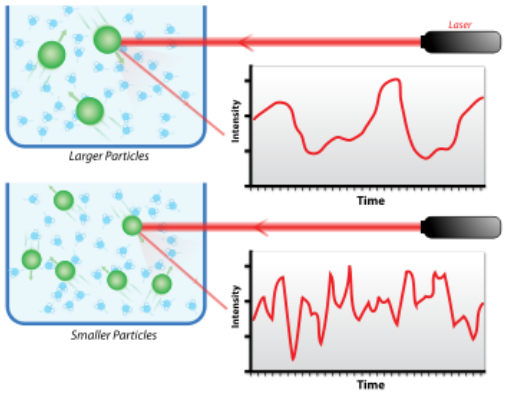


**Pic. 6:** Dynamic light scattering of different sizes of particles and their signal [35].

DLS was used for measuring the diameter of Ag-NPs produced in different conditions. For measurement was used quartz cuvette and disposable polystyrene cuvettes. Typical time of acquisition was 10 – 15 s and 10 acquisitions were measured for obtaining one measurement. Every sample was measured at least 3 times. For evaluation of results was used program Dynamics by Wyatt technology.

### 2.3.3 Rheometry and rheology

Rheology is a science discipline which studies deformations and flow of the matter. Flow properties of the polymers, melts, dispersions or solutions are important for their further processing. Material under applied forces can show two ideal types of behavior. Object responding with elastic deformation gains the same shape after removing external forces. Opposite example is viscous behavior in which external forces cause viscous flow but after removing forces object do not get the original shape. Energy causes deformation is dissipated to heat. Polymer materials response to applied stress is viscoelastic, having character both,

viscous and elastic components [36]. Measurement of flow properties is divided into linear and non-linear behavior.Viscosity is resistance of material to flow and it is caused by inner friction of fluid.

Rheology was measured in order to investigate changes in viscosity related to different ratios between HA/Ag-NPs and PVA, as viscosity of solution is important parameter for electrospinning. Viscosity of HA/Ag-NPs : PVA nanocomposite blend was measured by ARES G2 Rheometer by TA Instruments and results were processed by program Trios by TA Instruments. Cone to plate geometry with cone angle 2 ° and diameter of cone 40 mm was used for all samples. Approximately 0.62 ml of sample was used for one measurement and samples were diluted to concentration 1.8 mg/ml. Both steady flow test and oscillation test were carried out for all samples.

## 2.4 Characterization of nanofibers

### 2.4.1 Scanning electron microscopy (SEM)

The scanning electron microscopy uses focused beam of high-energy electrons to generate various signals at the surface of solid specimens. Accelerated electrons can pass through the sample or undergo either elastic or inelastic scattering. Elastic and inelastic scattered electrons result in many signals which are used for SEM imaging. Typical signals are secondary electrons, backscattered electrons, cathodoluminescence, auger electrons and characteristic X-rays. SEM provides information about external morphology (texture), chemical composition, and crystalline structure of material. Areas ranging from 1 cm to 5 μm in width can be imaged using magnification from 20 x to approximately 30 kx. It is especially useful for qualitative or semi-quantitative determining of chemical composition using Energy-Dispersive X-Ray spectroscopy (EDS). The name scanning has SEM due to obtaining picture pixel by pixel acquiring signal of electrons from the particular part of specimen.

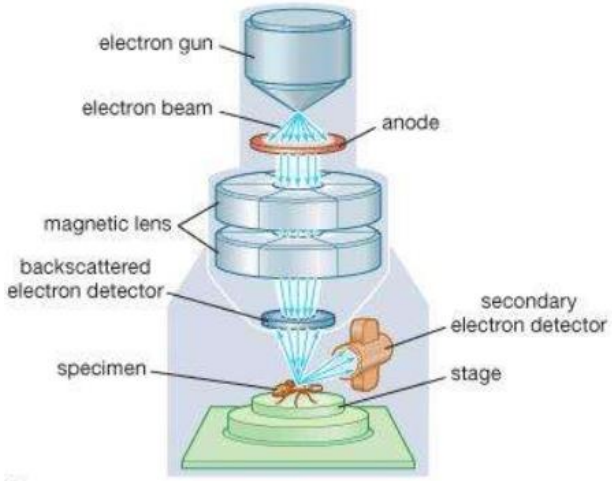


**Pic. 7** Scheme of Scanning electron microscope [37].

EDS system, typically integrated in SEM instrument, include x-ray detector mounted in the sample chamber. Detector contains Si(Li) crystals that absorb the energy of incoming x-rays by

ionization and free electrons in the crystal that become conductive produce electrical charge bias. X–ray absorption is proportional to voltages and electrical pulses correspond to the characteristic x–rays of element [38].

In this research SEM was used for imaging of morphology of nanofiber sheets and further analysis of the diameter of nanofibers. EDX was used for elemental analysis of nanofibers. Nanofiber sheets were coated with the thin conductive layer of Pd/Au mixture before studying by SEM. Both the imaging of nanocomposite surface and EDX analysis was carried out for each sample. Imaging of morphology was obtained at magnifications 1 kx, 5 kx, 10 kx, 20 kx, 35 kx, 75 kx, 200 kx.

### 2.4.2 Transmission electron microscopy (TEM)

Transmission electron microscope uses accelerated electrons passing through the sample to create image with resolution around 0.1 nm. As electron beam passes through the sample, particles of the sample modify it and imprint its image in detector. Absorption only play a minor role, diffraction phenomenon is essential. Beam of electron is usually produced by tungsten filament due to its relatively low work function making it comparatively easy to emit electrons from tungsten surface. Filament and surrounding fun elements of microscope are held at high negative potential, electrons are accelerated away from filament. Source, gun and column of microscope are at high vacuum otherwise would be electrons scattered by atoms [39]. Condenser lenses gather electrons and focus them onto the specimen to illuminate only area being examined. Objective lens focuses and initially magnify image. As detector for TEM is usually used phosphorescent screen, emitting photons when irradiated by the electron beam [40]. Sample with thickness less than 100 nm should be used wherever it is possible, for some applications even less than 10 nm [41].

There are two imaging modes in TEM, image observation mode and diffraction image operation mode. In conventional TEM is used image observation mode which detects electrons that passed through sample. In diffraction image operation mode diffracted electron beam is projected onto the screen by imaging lenses [39].

TEM investigations were performed employing the JEOL JEM-2010 (HT) electron microscope (JEOL, Japan), with the accelerating voltage of 120 kV. The sample was diluted in milli-Q water with concentration of 0.5 mg/ml, and a drop was placed on Cu grids pre-coated with carbon films and air dried.

### 2.4.3 Fourier-transform infrared spectroscopy (FTIR)

Fourier-transform infrared spectroscopy is spectrophotometric method using radiation with wavelengths of 4000 ~ 400 $cm^{-1}$ for analyzing organic compounds and inorganic ions. Irradiated molecules absorb selectively at different wavelength, which cases the change of dipole moment of sample molecule. In these molecules are vibrational energy levels transformed from ground to excited state. The number of absorption peaks depends on number of vibrational freedom of the molecule and intensity of peak is related to the change of dipole moment of molecule. It means that only molecules with the change of dipole moment absorb in IR spectra [42]. Absorption occurs when frequency of IR radiation has the frequention of vibration of molecule

or chemical group. FTIR consist of IR source, interferometer, sample compartment, detector and computer. Compared to conventional IR spectrophotometer it does not have monochromator and the main part of it is interferometer. Interferometer splits the beam of light, so the paths of two beams are different. In detector is difference in intensity of two beams measured as a function of the difference of the paths. Measuring of all the frequencies simultaneously makes from FTIR quick measurement. It has also higher sensitivity and is mechanically simple when compares with dispersive technique. In attenuated total reflection (ATR) mode multiple reflection from Ge, diamond, ZnSe or Si crystal gives more intensive spectrum, but close contact with crystal is fundamental. ATR is suitable for measurement of solid and liquid samples [43].

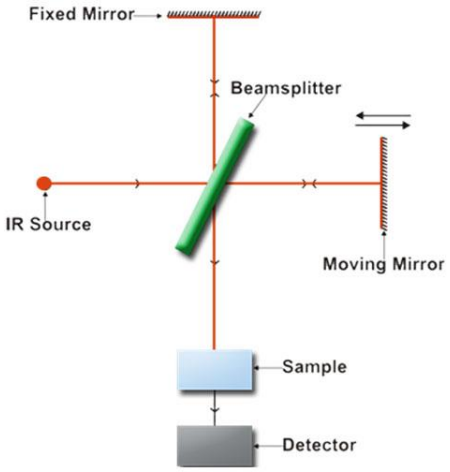


**Pic. 8:** Schematic picture of FTIR [44].

FTIR was carried out in order to prove functional groups in produced nanofiber sheets and discovering possible differences from pure nanofiber materials. ATR mode was used for all samples.

### 2.4.4 Thermogravimetry analysis (TGA)

Thermogravimetry analysis is technique which measure weight as function of temperature while is sample undergoes defined temperature program. Specimen could be either heated or cooled and temperature changes could be provided in different rates. There could be studied decomposition by temperature in different atmospheres such as an air or nitrogen atmosphere. Sample is usually solid or more rarely liquid. Output from thermogravimetry measurement is thermogravimetric curve, providing information about thermal stability, oxidative mass losses, thermogravimetric kinetics, humidity of the sample or composition of the sample. Alternative to the thermogravimetric curve is derivative thermogravimetric curve (DTG) presenting rate of change of mass dependent on temperature or time. Conventionally is TGA carried out at constant heating rate as the function of time [45].

TGA in this case was used for study of thermal stability and moisture content of different composition of wound dressing sheets. Measurement was carried out in the inert nitrogen with temperature rate 10 °C/min up to 800 °C. Weight of the samples was 5 µg and alumina pan was used for all samples.

### 2.4.5 X-Ray Diffraction (XRD)

X-Ray Diffraction is rapid analytical technique used for study pf crystal structures and atomic spacing. XRD is based on the knowledge that X-ray wavelengths are similar to the spacing of the planes in a crystal lattice, thus X-Rays are diffracted by crystal structures. There is constructive interference between monochromatic X-rays and crystalline sample when conditions satisfy Bragg´s Law ($n\lambda = 2d \sin\theta$) [46].

X-ray diffraction was measured at 3 kW diffractometer Smart lab from Rigaku using Cu Kα radiation (λ = 1.54 Å) and detector Dtex Ultra with Bragg-Brentano geometry. Diffraction angle 2-Theta was measured in range from 5° to 80° with step size 0.02° at speed 4°/min. Generator was operated at current 30 mA and voltage 40 kV.

### 2.4.6 Tensile testing

Tensile test or tension stress is one of the fundamental type of mechanical tests. It is performed by pulling specimen in one axis, tracking the change in stress as function of constantly increasing strain. Output from measurement is stress-strain curve which determines useful parameters as strength at break, elongation at break and it is further possible to count Young´s modulus from it.

Tensile testing was used for investigation of strength of nanofiber sheet which is important when it comes to handling wound dressing. It was carried out by Universal testing equipment ZWICK Z 010 from Zwick – Roell with 10 N measuring cell. Samples were cut to the dogbone shape with parallel specimen length 10 mm. Testing speed was 5 mm/min.

**Pic. 9:** Tensile testing of HA/Ag-NPs nanocomposite material with ZWICK Z 010, Zwick – Roell, 10 N measuring cell.

# 3. RESULTS AND DISCUSSION

### 4.1. Preparation of nanocomposite (HA/Ag-NPs)

Silver nanoparticles were prepared by *in-situ* way (chemical reduction) using sodium hyaluronate (HA) as reducing and capping agents. Three main steps should be evaluated from the green chemistry perspective for preparation of nanoparticles. Choice of the solvent medium used for synthesis, choice of environmentally benign reducing agent and choice of nontoxic stabilizing agent for NPs stabilization [47]. In order to fulfill these requirements, demineralized water was used as solution and hyaluronan was used as both reducing, and stabilizing agent at the same time.

Firstly, the certain concentration of HA (1, 2 %) was dissolved in milli-Q water at room temperature, the different concentrations of silver nitrate ($Ag^{+}$) were used as a source of silver nanoparticles ($Ag^{0}$; 0.01, 0.1, 0.3, 0.5 and 1 M). The pH of the reaction medium was raised using sodium hydroxide (2 M). No toxic external reducing agent such as sodium borohydride, hydrazine hydrate, *N, N* – dimethyl formamide was used for the reduction of $Ag^{+}$ to $Ag^{0}$. The color of the reaction mixture changed from colorless to yellowish – yellowish brown (depends on concentration of used $Ag^{+}$) color indicated formation of *in-situ* Ag NPs. Fig. 1 shows the UV/Vis spectroscopy of hyaluronan/ silver nanoparticle composite (HA/AgNPs) using 1 % HA; 0.01 M $Ag^{+}$ (1 ml) at different reaction time (10 – 60 min). The absorption peak of $Ag^{0}$ (410 nm) was attributed to surface plasmon resonance of the colloidal silver nanoparticles, which indicated that the silver in HA/Ag-NPs nanocomposite exists in the form of nanoparticles. As we can see the intensity of $Ag^{0}$ (410 nm) was decreased by increasing the time of reaction from 10 to 60 min. The right side of Fig. 1, shows the optical pictures of HA/Ag-NPs after different reaction time. There were not significant changes of color according to change of the reaction time.

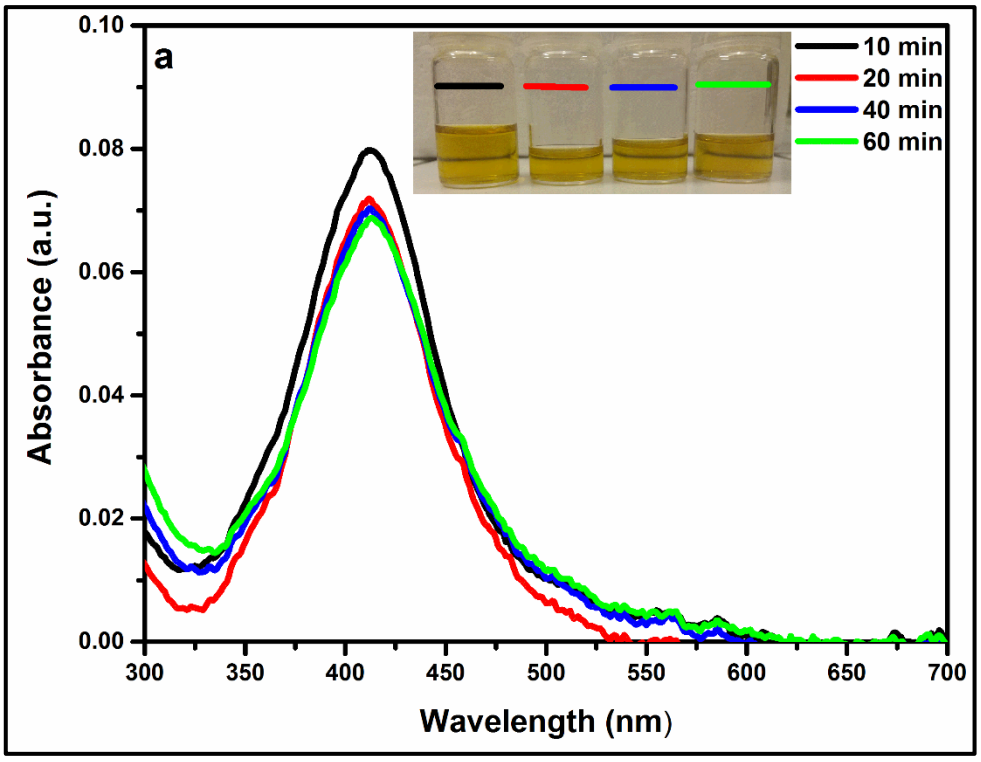


**Fig. 1:** Representative the UV/Vis spectra of HA/AgNPs nanocomposite

**Experimental conditions**: 1 % HA, 0.01 M $AgNO_3$, 1 ml NaOH, 90 $^0$C and 10 times diluted

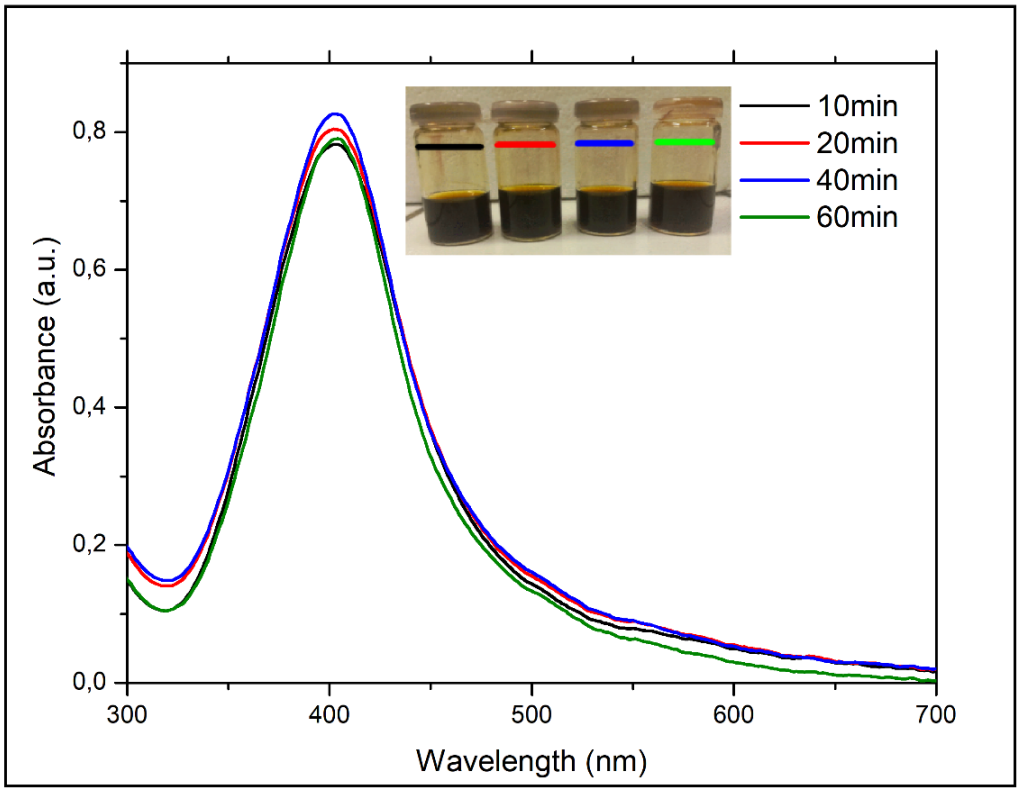


**Fig. 2:** UV/Vis spectra of HA/AgNPs nanocomposite synthesized at different time

**Experimental conditions:** 1 % HA, 0.1 M AgNO3, 1 ml NaOH, 90 0C and 10 times diluted.

Fig. 2 presents the UV/Vis absorption spectra of HA/Ag-NPs using 0.1 M Ag+ at different time with constant concentration of HA (1 %), temperature of the reaction was 90 °C. Notably, Ag-NPs were prepared and the peak related to $Ag^0$ was visualized at 410 nm, and there was not any peak related to silver ions around 350 nm, which confirmed that all silver ions were reduced to silver nanoparticles. Sample with 0.1 M $Ag^+$ showed increasing slight trend of time dependence of absorbance with highest absorbance at 40 minutes.

It could be observed from Fig. 3 and Fig. 4 that after using higher concentration of $Ag^+$ (0.5 M and 1 M ) there was not any peak related to silver ion, only after 10 min of reaction slightly broad peak appeared at 350 nm, and then disappeared with increasing time of reaction. Peak at 280 nm appeared with increasing time of reaction (Fig. 3 and Fig. 4 green line). From the results of Fig. 3, it could be conclude that, concentration above 0.1 M of silver nitrate cannot be used for preparation of Ag-NPs using hyaluronan, in this case.

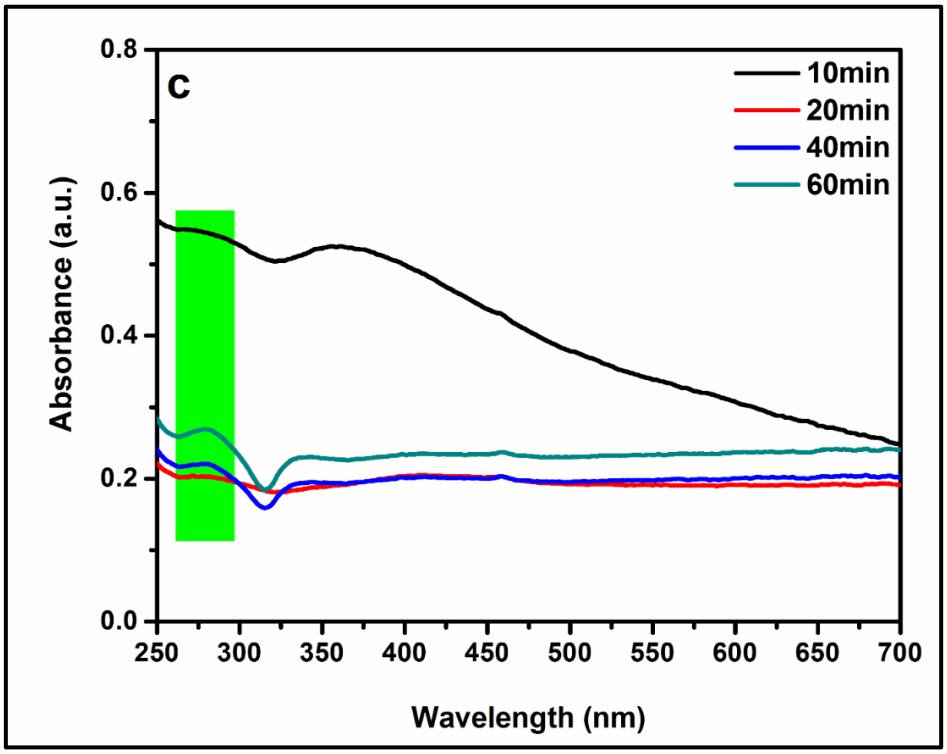


**Fig. 3**: UV/vis spectra of HA/AgNPs nanocomposite synthesized at differnt time

**Experimental conditions**: 1 % HA, 0.5 M $AgNO_3$, 1 ml NaOH, 90 $^0$C and 10 times diluted

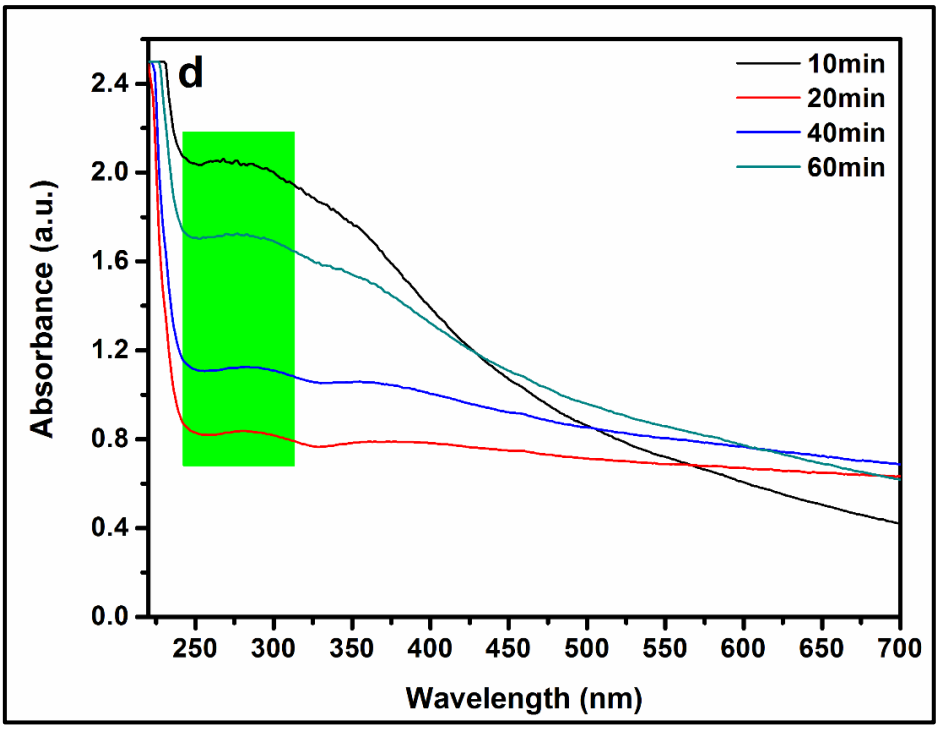


**Fig. 4:** UV/Vis spectra of HA/AgNPs nanocomposite synthesized at different time

**Experimental conditions**: 1 % HA, 1 M $AgNO_3$, 1 ml NaOH, 90 $^0$C and 10 times diluted

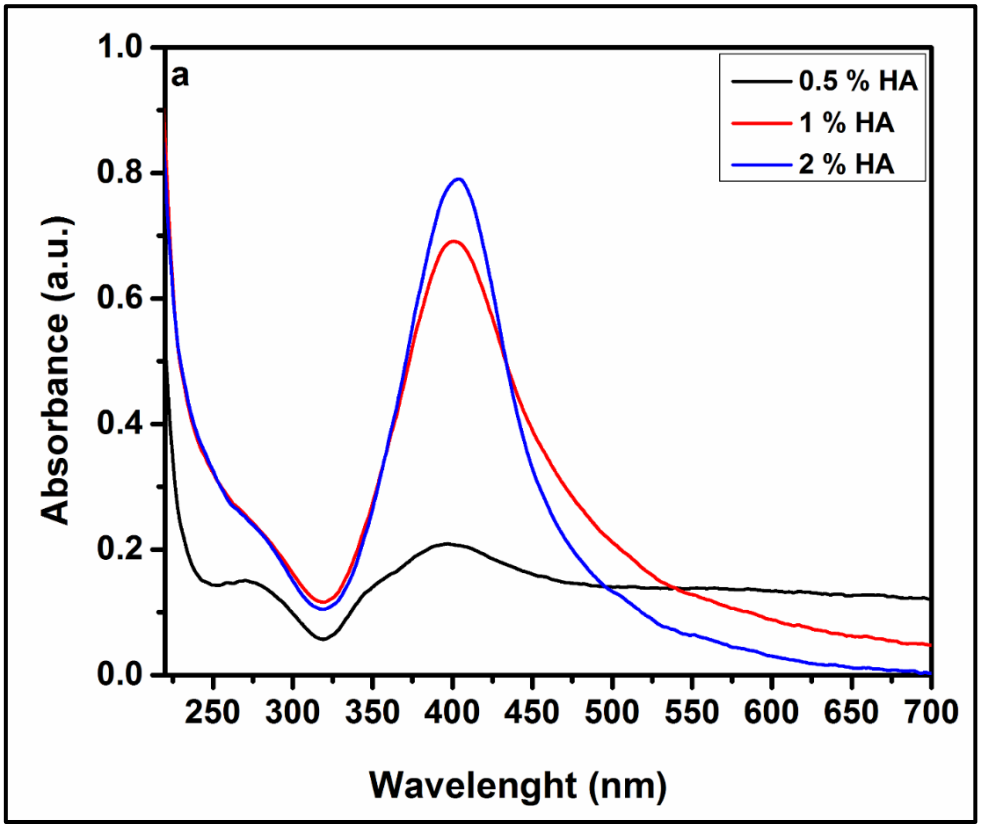


**Fig. 5:** UV/Vis of hyaluronan/Ag-NPs nanocomposite using different concentration of hyaluronan

**Experimental conditions**: 0.1 M AgNO3, 1 ml NaOH, 90 °C and 10 times diluted with different concentration of hyaluronan (0.5, 1, and 2 %).

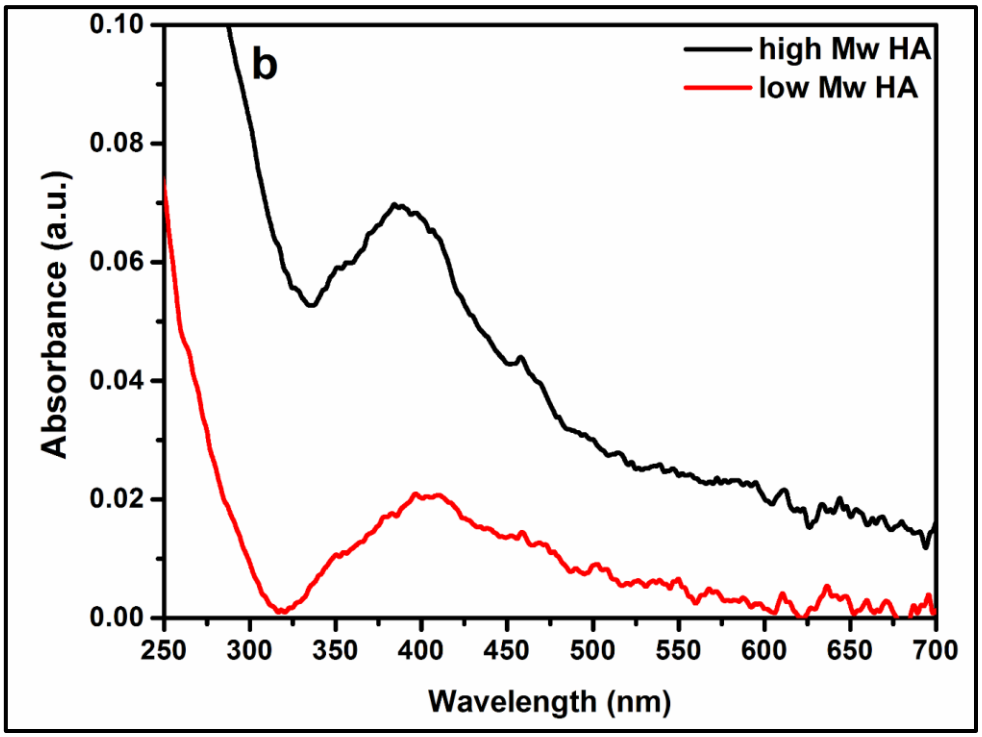


**Fig. 6:** UV/Vis spectroscopy of HA/Ag-NPs nanocomposite using different molecular weights of HA

**Experimental conditions**: 1 % HA; 0.01 M $AgNO_3$, 1 ml NaOH, 10 times diluted solution, lower and higher Mw of HA.

Fig. 5 shows the UV/vis spectroscopy of different concentrations of hyaluronan used for preparation of the silver nanoparticles. The intensity of absorption peak of $Ag^0$ was increased significantly by increasing the concentration of HA, this may happened due to the higher presence of carboxylic groups that could interact with silver nanoparticles (physically or chemically) bonded, and by increasing the carboxylic content the absorption peak of Ag was increased. 0.5 % HA in Fig. 5 was in not enough for full reduction of silver ions to the silver nanoparticles and still remained small amount of silver ion related to the peak appeared at 280 nm. This may be due to the fact that with the decrease of HA content, fewer Ag+ was reduced and few HA molecules absorbed on the pre-formed particles resulting in the formation of large Ag clusters. Based on the results from Fig. 5, concentrations (1, 2 %) hyaluronan was enough for complete reduction of Ag+ to $Ag^0$, but 0.5 % HA was not enough. Two different molecular weights were used for fabrication silver nanoparticles (low and high) as could be seen in Fig. 6 higher molecular weight has higher reducing power than lower molecular weight and the absorption peak related to $Ag^0$ was higher comparing with low Mw HA (Fig. 6). The content of hyaluronan in the reaction system could also affect the reduction of silver ion to silver nanoparticles. For best results of this study is optimal high MW of HA due to its higher ability to reduce $Ag^+$ ions to $Ag^0$ what could meet with its higher ability to heal wounds than low MW HA proved on *in-vivo* tests in research of Fouda et al. [25] to produce optimal wound dressing.

The effect of concentration of hyaluronan (2 %) using different concentrations of silver nitrate was investigated in Fig. 7 which shows the effect of reaction time on the reduction rate of silver by UV/Vis spectroscopy while keeping the temperature, concentration of HA and pH = 11 for different time (10 – 60 min) with 0.01 M Ag+. Higher absorption occurred after 20 minutes of reaction. When the time of reaction was higher than 20 minutes, another peak appeared at 280 nm, related to silver ion. Fig. 8 represents the UV/Vis absorption spectra of HA/Ag-NPs (2 % HA, 0.1 M) prepared at different times of reaction.

The data reveal several important findings which could be presented as follows: (i) at the early stage reaction duration (after 5 min, data not shown) the plasmon band was broaden and simple test for silver ion using NaCl solution indicates low conversion of $Ag^{+}$ to metallic $Ag^{0}$ at this time, (ii) prolonging the reaction duration up to 20 min leads to outstanding enhancement in the plasmon intensity indicating that large amounts of silver ions were reduced and used for cluster formation, (iii) further increase in the reaction duration up to 40 min is accompanied by marginal decrement in the absorption intensity which could be attributed to some aggregation of the formed silver nanoparticles, (iv) increasing the reaction duration up to 60 min leads to significant decrease in the absorption intensity.

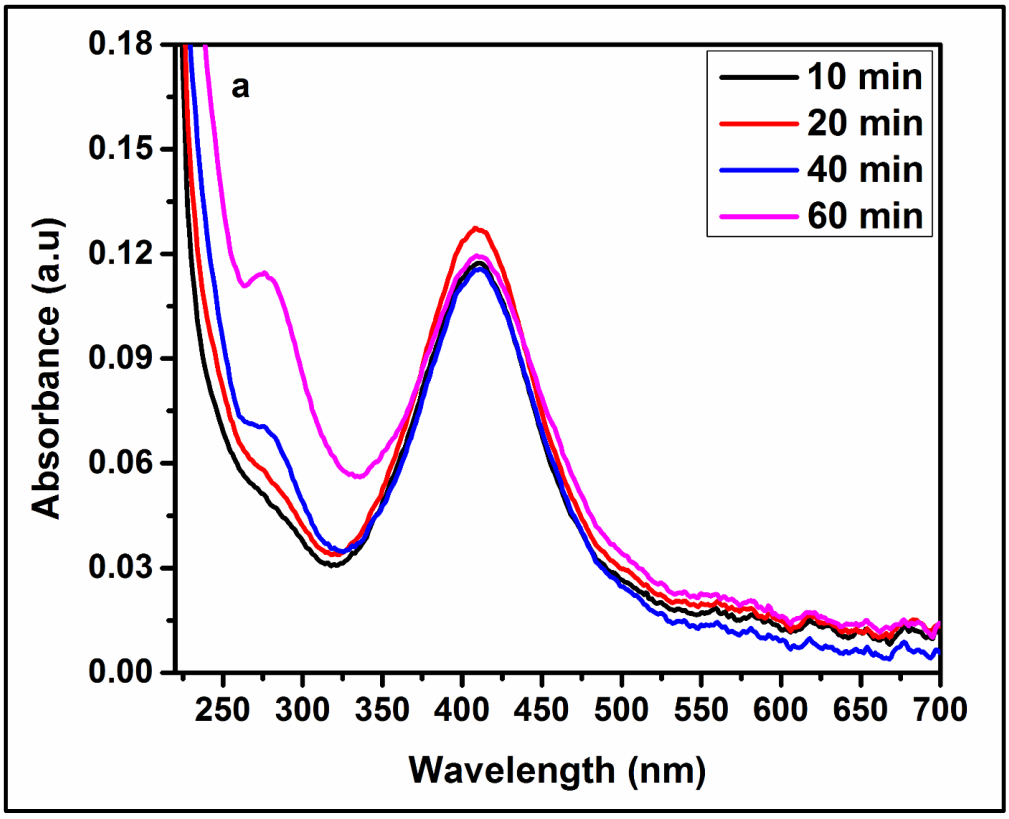


**Fig. 7:** UV/Vis spectra of HA/Ag-NPs nanocomposite using 2 % HA

**Experimental conditions**: 2 % HA, 0.01 M $AgNO_3$, 1 ml NaOH, 90 $^{0}$C and 10 times diluted

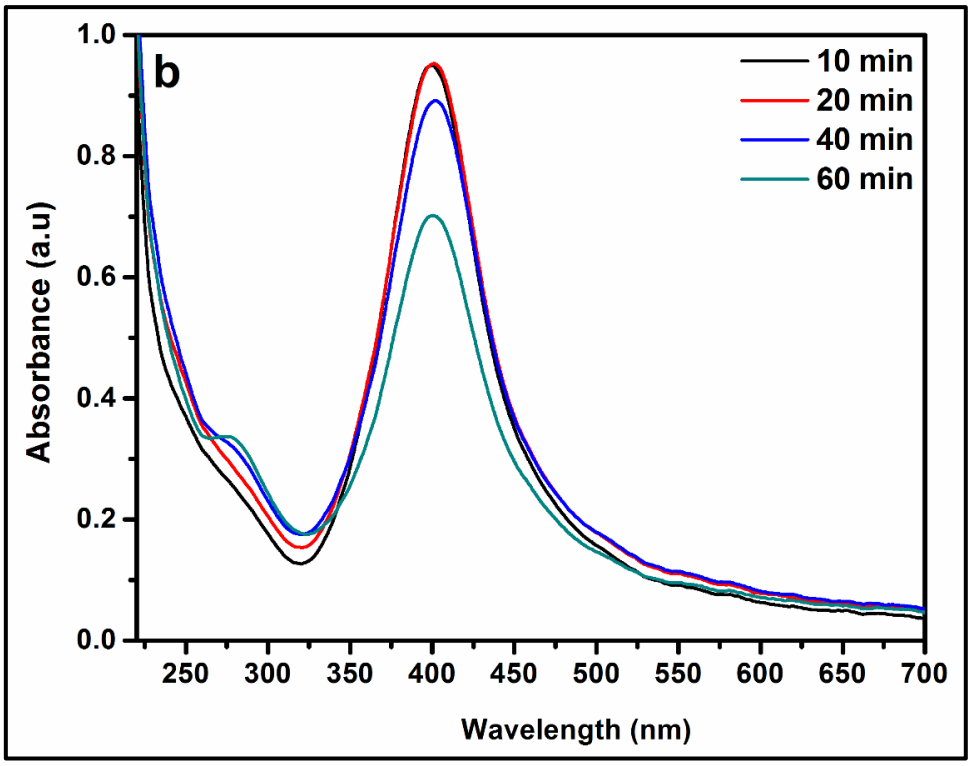


**Fig. 8:** UV/Vis spectra of HA/Ag-NPs nanocomposite using 2 % HA

**Experimental conditions**: 2 % HA, 0. 1 M $AgNO_3$, 1 ml NaOH, 90 $^0$C and 10 times diluted

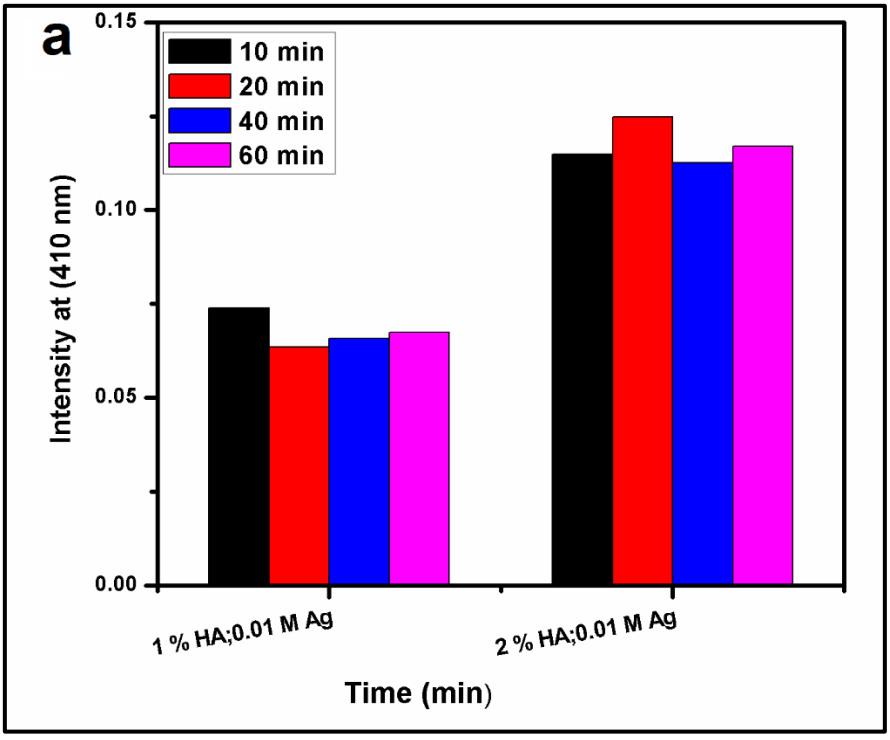


**Fig. 9**: Time dependence of UV/Vis absorbance in different concentration of HA

**Experimental conditions**: HA (1, 2 %), 0. 01 M $AgNO_3$, 1 ml NaOH, 90 $^0$C and 10 times diluted

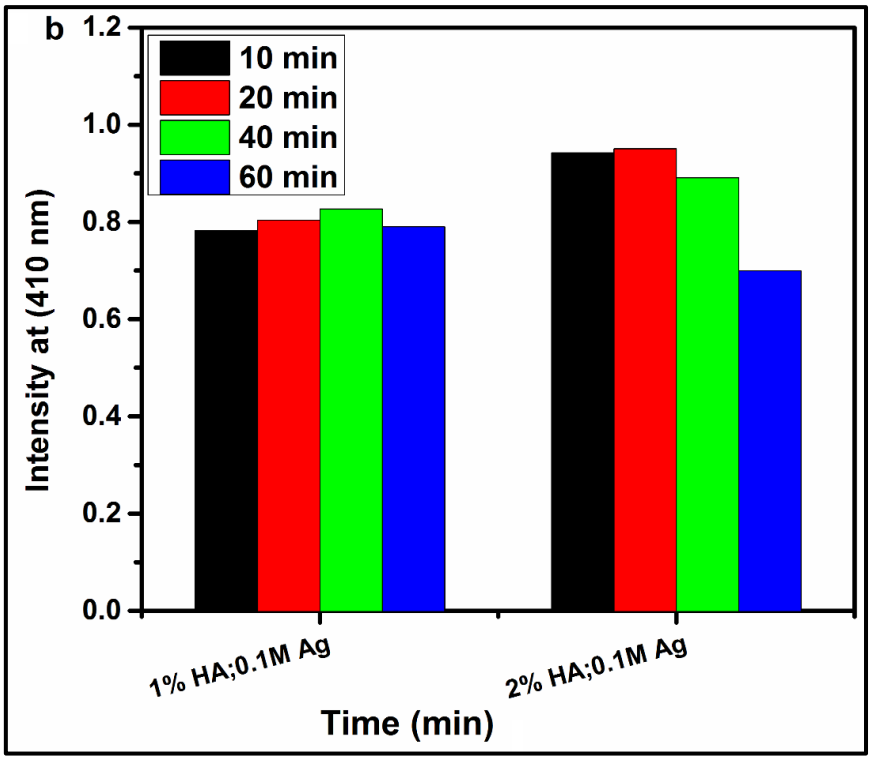


**Fig. 10:** Time dependence of UV/Vis absorbance in different concentration of HA

**Experimental conditions**: HA (1, 2 %), 0. 1 M $AgNO_3$, 1 ml NaOH, 90 $^0$C and 10 times diluted

Time dependence of UV/Vis spectroscopy at absorption peak of Ag at 410 nm revealed that the absorbance was the highest after 20 minutes of reaction for samples 2 % HA, 0.01 M and 0.1 M what can be more clearly seen in Fig. 9 and Fig. 10. In samples with 1 % HA absorbance varies in range of one hundredth. Absorbance dropped more significantly with time only in sample 2 % HA, 0.1 M $Ag^+$. Basically, UV/Vis absorption did not vary a lot after different times of reactions, there was conformity in the highest absorbance (20 minutes) in two samples. Fig. 11 shows the effect of volume of sodium hydroxide (50 and 100 µl) on preparation of $Ag^0$ with constant concentration of hyaluronan and silver nitrate 1 % and 0.1 M, respectively. There was small peak for AgNPs that is lowering with time of reaction. However, there is still significant peak for $Ag^+$ ions from silver nitrate located around 280 nm, what indicates that volume of NaOH was too low for activation the functional groups of HA; thus, there was not enough reduction agent for $AgNO_3$ and there are still some $Ag^+$ ions present in the solution.

According to results from UV/Vis spectroscopy, solution with 1 % HA; 0.1 M $Ag^+$ and solution 2 % HA; 0.1 M $Ag^+$; were chosen to continue with to further characterization.

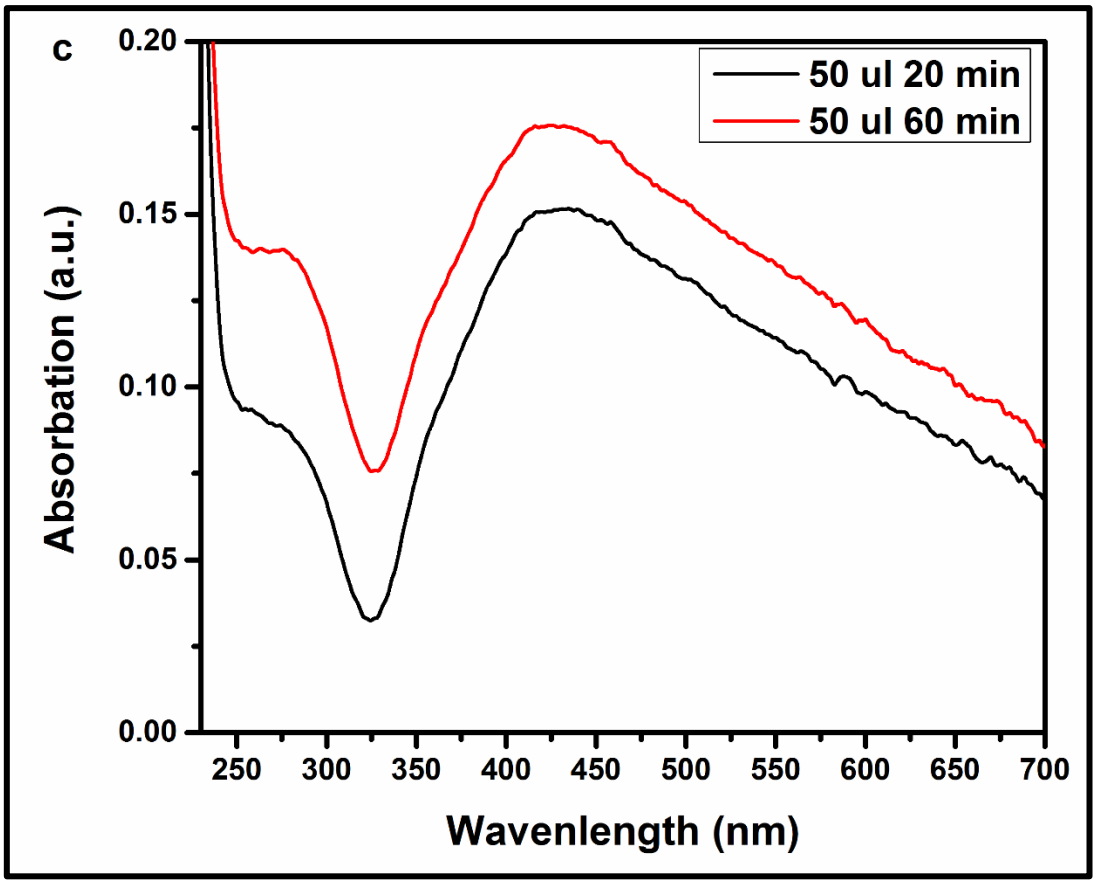


**Fig. 11**: Time dependence of UV/Vis absorbance using lower volume of sodium hydroxide

**Experimental conditions**: HA (1 %), 0. 1 M $AgNO_3$, 50 µl of NaOH, 90 $^0$C, different reaction time 20 and 60 min, 10 times diluted

### 3.2 Particle size of silver nanoparticles

According to UV/Vis spectroscopy results, synthetized Ag-NPs were present in noticeable quantities only in samples with lower concentration, i.e. 0.01 M and 0.1 M $Ag^+$. In these samples, diameter of nanoparticles in nanocomposite was determined by two different techniques, DLS and TEM. According to DLS results, shown in Fig. 12, the average diameter increased from 1.2 ± 0.12 nm to 2.4 ± 0.28 nm (radius 0.6 ± 0.06 nm to 1.2 ± 0.14 nm). Seemingly, there could be connection between concentration of $Ag^+$ and size of NPs, as the band for samples with 0.1 M $Ag^+$ was slightly shifted to the larger values of radius, than samples with 0.01 M $Ag^+$, what corresponded with results from the previous study [48] which related higher concentrations of $Ag^+$ with synthesis of bigger particles and formation of agglomerates.

Particle size distribution was narrower for samples with 2 % HA; however, this could be partially influenced by the use of different cuvette (wide window cuvette) for 2 % HA which was chosen as it better suits the character of the samples.

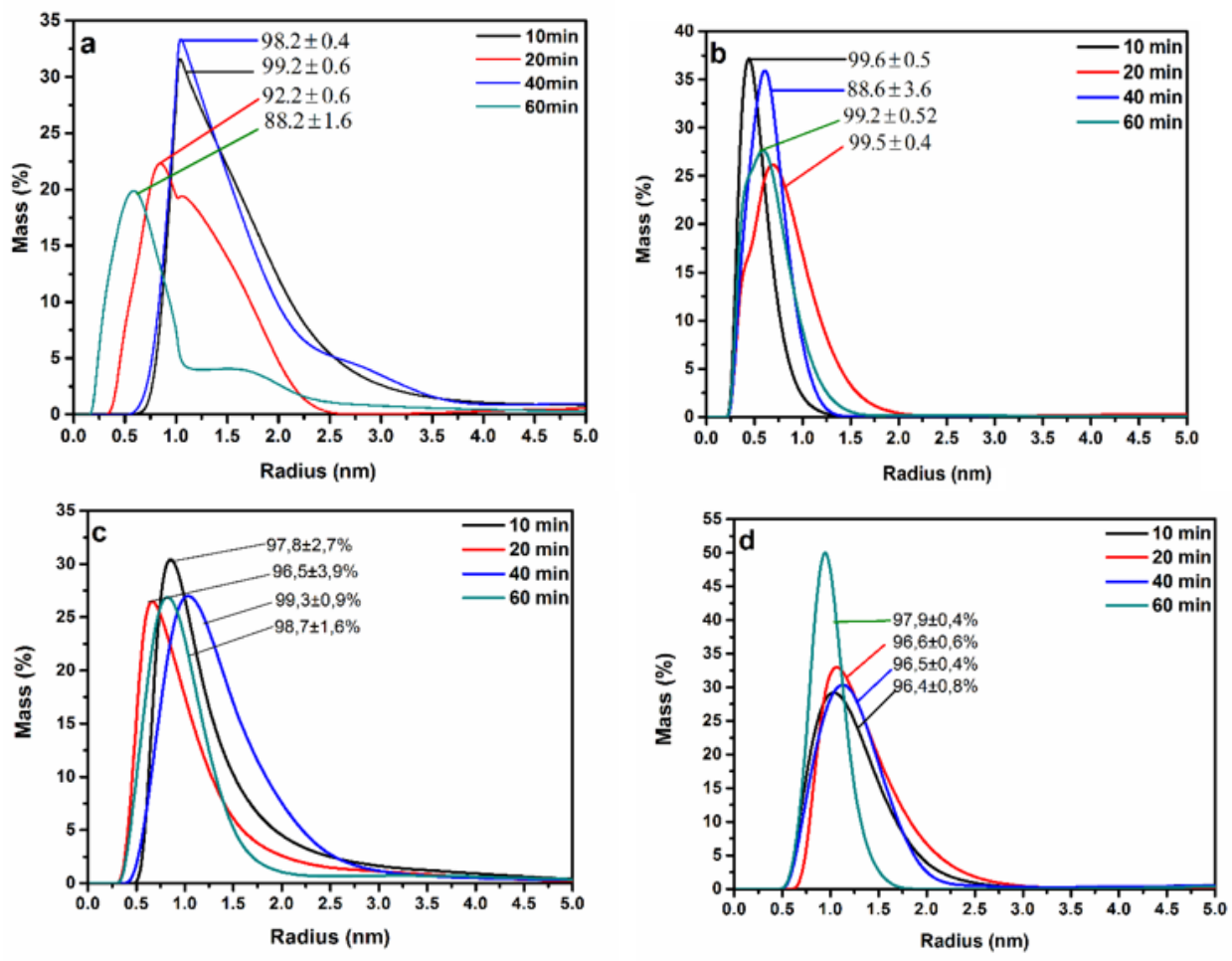


**Fig. 12:** DLS of nanocomposite (HA/Ag-NPs) using different concentrations of HA and Ag+

**Experimental conditions:** a) 1 % HA, 0.01 M Ag+; b) 1 % HA, 0.1 M Ag+; c) 2 % HA, 0.01 M Ag+; d) 2% HA, 0.1 M Ag+

### 4.3. TEM of the HA/Ag-NPs nanocomposite

Fig. 13 shows images made by the transmission electron microscopy (TEM) of nanocomposites HA/Ag-NPs where nanoparticles were fabricated using hyaluronan (1 %), 0.1 M silver nitrate, prepared at different times of reaction. It represents the TEM and particle size distribution histogram of HA/Ag-NPs nanocomposite prepared after 10, 20, 40 and 60 min. TEM images shows well distribution of spherical silver nanoparticles. The corresponding size distribution histogram clearly illustrates the Ag-NPs prepared at different time (10 – 60 min) and the average size of the formed particles seem to be in the range from 2.5 to 7 nm (10, 20,40 min; Fig. 13 a, b, c), then the size of Ag-NPs were increased with the time (3 nm – 7.5 nm; Fig. 13 f, h) after 60 minutes.

### 4.4. Rheological properties of HA/Ag-NPs nanocomposite

After finding out the best parameters of HA/Ag-NPs nanocomposite, this solution was blended with PVA solution to prepare different ratios between PVA and HA/Ag-NPs suitable for electrospinning. Viscosity is a very important parameter when it comes to electrospinning. More ratios between HA/Ag-NPs composite and PVA were tested. As the viscosities of different ratios varied over one order of magnitude from dilute to fairly viscous, both steady flow and oscillation tests were carried out for all samples. Notably, steady flow is more suitable for low-viscosity samples while oscillation tests provide better quality results for more viscous solutions.

Sample 1 % HA, 0.1 M $Ag^+$ and 2 % HA, 0.1 M $Ag^+$ were mixed with 16 % solution of PVA in ratios 50:50, 40:60, 20:80, 90:10, 95:5, respectively. Viscosity of PVA and HA was measured as well. Fig. 14 shows the results from the both steady flow viscosity and oscillation complex viscosity tests. The observable non-linearities were attributed to flow instability and inertia effects rather than a genuine non-Newtonian behavior; thus, the samples were considered Newtonian throughout the investigated shear rate range.

Fig. 15 directly compares the results of both steady flow viscosity and oscillation complex viscosity according to the empirical Cox-Merz rule showing no significant differences between these two measuring modes; hence, despite all samples were studied by both rheology modes, the final results in Fig. 15 b were composed from only a single type of data per sample depending on its viscosity and the quality of the collected data. For less viscous solutions of HA/Ag-NPs : PVA (pure HA, 50:50, 40:60) results from flow test have been used while for more viscous solutions (80:20, 90:10, 95:5, pure PVA) have been used results from oscillation tests. There is over a 20-fold increase in viscosity with increasing concentration of PVA present in measured solution.

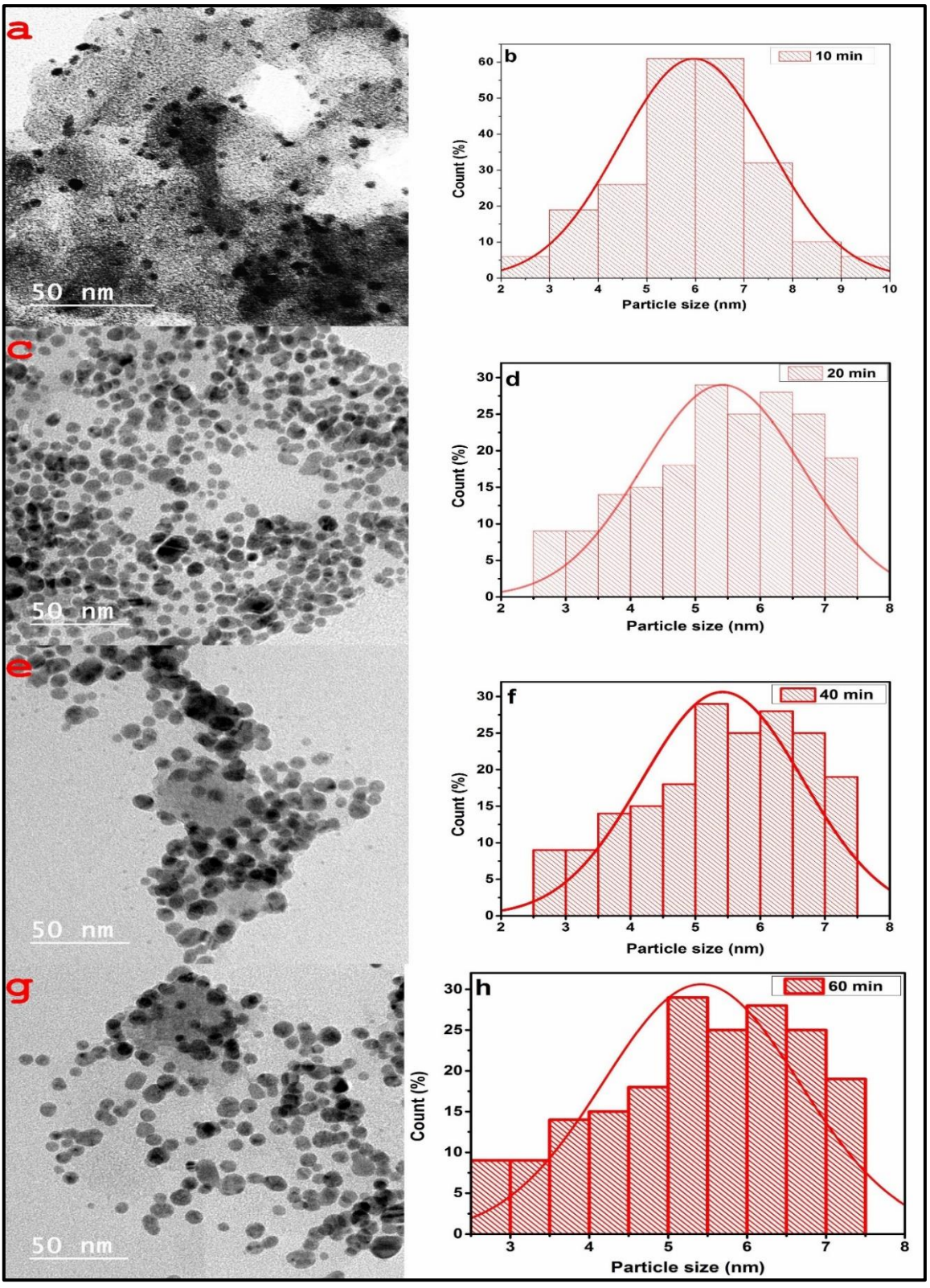


**Fig. 13:** Representation of the TEM and histogram of HA/Ag-NPs nanocomposite

Experimental conditions: a) 1 % HA, 0.1 M Ag+, 1 ml NaOH, 10 min; b) histogram of 1 % HA, 0.1 M Ag+, 1 ml NaOH, 20 min; C) 1 % HA, 0.1 M Ag+, 1 ml NaOH, 20 min; d) histogram of 1 % HA, 0.1 M Ag+, 1 ml NaOH, 40 min, e) 1 % HA, 0.1 M Ag+, 1 ml NaOH, 40 min; f) 1 % HA, 0.1 M Ag+, 1 ml NaOH, 60 min; g) 1 % HA, 0.1 M Ag+, 1 ml NaOH, 20 min; g) 1 % HA, 0.1 M Ag+, 1 ml NaOH, 20 min; h) histogram of 1 % HA, 0.1 M Ag+, 1 ml NaOH, 60 min.

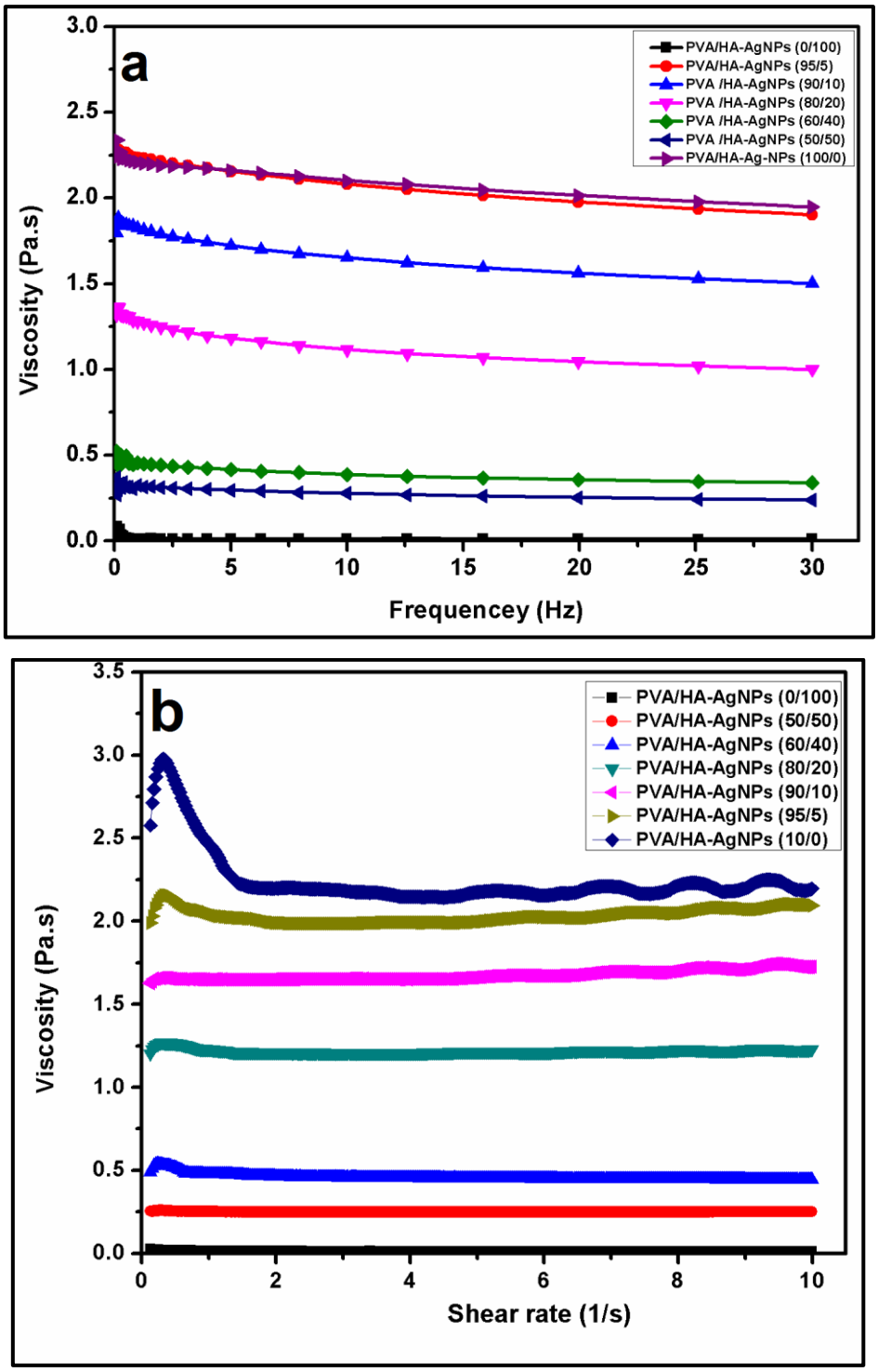


**Fig. 14:** *Rheological properties of the PVA/HA-Ag-NPs nanocomposites*

**Experimental conditions:** a) Flow test – viscosity dependence on shear rate (note the measurement artefact pronounced for more viscous samples), using different ratio between PVA and HA/Ag-NPs at room temperature; b) Oscillation test – complex viscosity dependence on frequency using different ratio between PVA and HA/Ag-NPs at room temperature.

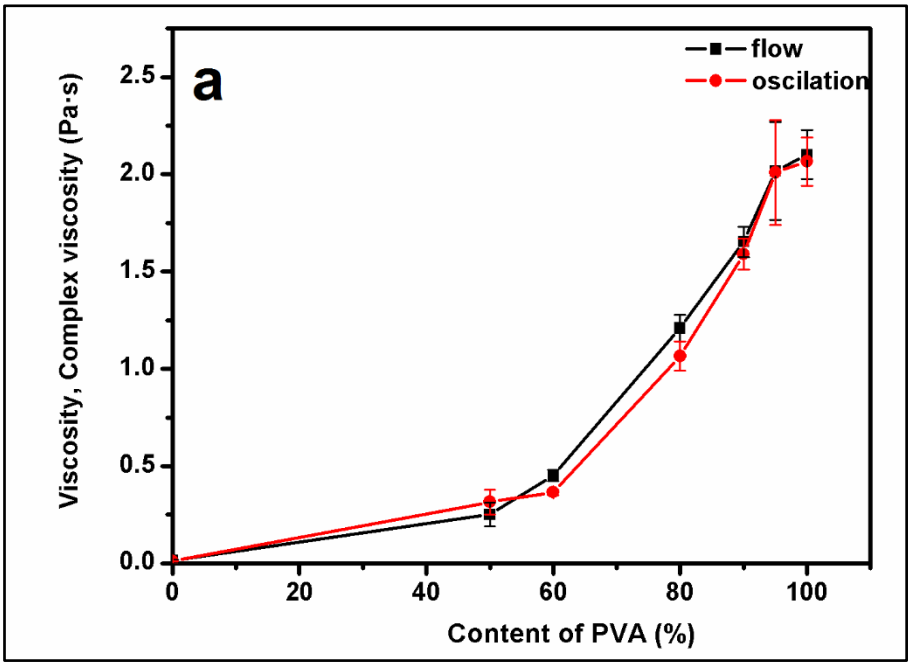


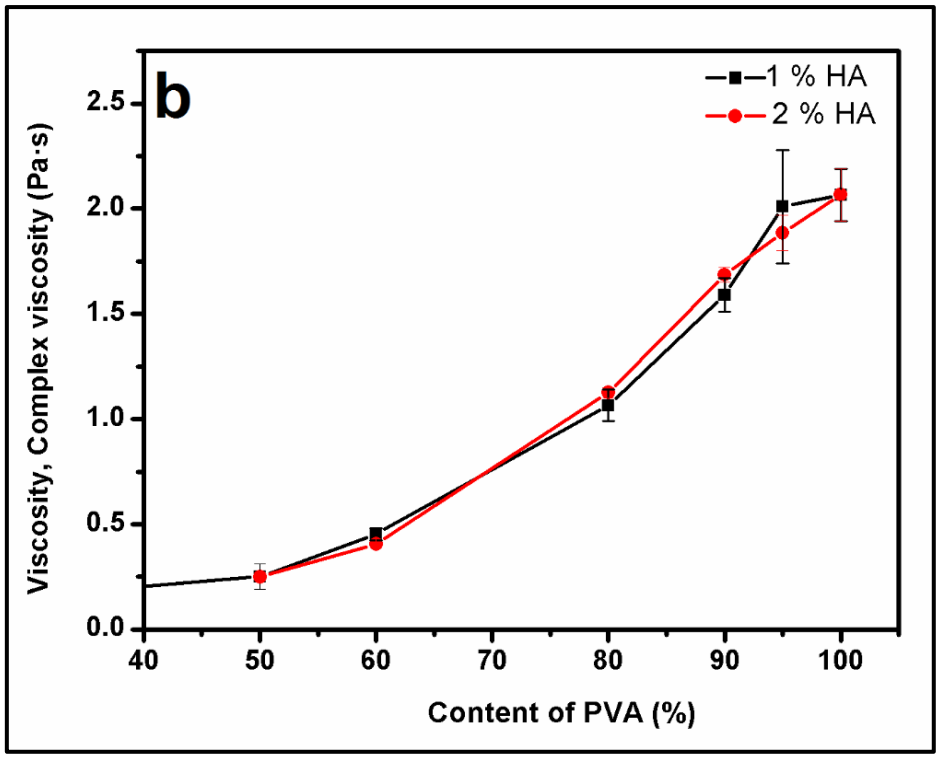


**Fig. 15**: Comparison of flow and oscillation rheology with different ratio of PVA to HA/Ag-NPs: PVA, with standard deviation bars (a); comparison of the viscosity of nanocomposite prepared by 1 % HA and 2 % HA, (b) with standard deviation bars (n = 30).

**Experimental conditions**: tested sample 1 % HA, 0.1 M Ag+, 16 % PVA; 2 % HA, 0.1 M Ag+, 16 % PVA; reaction time 20 min, different ratios of HA/Ag-NPs nanocomposite: PVA

### 4.5. Fabrication of PVA/HA-Ag-NPs wound dressings

Fabrication of nanofibers using hazard toxic solvents like tetrahedron furan, THF, chloroform, dimethyl formamide/Dioxane mixture, dichlor methane, formic acid, toluene, fluorinated compound derivatives and high concentration of acetic acid, etc., has limitation of the nanofiber applications in the medical field. For fabrication of nanofibers in this study, only pure water was used as a solvent. The best preparation conditions of hyaluronan-based AgNPs were used to produce nanofiber mats via electrospinning. Hyaluronan itself was difficulty fabricated by the electrospinning process using the regular solvents because of its polyanionic nature in solution. To overcome this short coming of hyaluronan, many researchers have sought to improve its electrospinning ability by mixing hyaluronan with other synthetic polymers such as poly(vinyl pyrrolidone) (PVP) , poly(ethylene oxide) (PEO), and poly(vinyl alcohol) (PVA). PVA has been also extensively used in this study to produce electrospun fiber mats with high mechanical integrity excluding use of hazard organic solvent such as DMF or mixture from DMF/and fluorinated solvent.

From the previous results (UV/Vis, TEM, rheology, and DLS), solutions of HA (1, 2 %), 0.1 M $Ag^+$, and reaction time 20 min were selected to continue with electrospinning. Therefore, PVA with special quality for electrospinning and concentration of 16 wt % was mixed with hyaluronan-AgNPs at various weight ratios (PVA/HA-AgNPs): 100/0, 95/5, 90/10, 80/20, 60/40, and 50/50 (Tab. 1). However, the viscosity was decreased in the case of PVA/HA-AgNPs blends, which may be attributed to the preparation procedure: During the reduction of $Ag^+$ ions in the preparation step hyaluronan may undergo degradation to certain extent due to the redox reaction and the heat treatment (Fig. 14 a).

**Tab. 1:** The composition of prepared nanocomposites and suitable electrospinning parameters

**Expermental conditions:** 16 % PVA; 1 % HA; 0.1M $Ag^+$; 20 min; mixed at RT, distance=130 mm, voltage 58 kV

| Sample labeling | Weight ratio between PVA and HA/Ag-NPs | Products |
|---|---|---|
| PVA/ HA-AgNPs | 100/0 | Nanofibers |
| PVA/ HA-AgNPs | 90/5 | Nanofibers |
| PVA/ HA-AgNPs | 90/10 | Nanofibers |
| PVA/ HA-AgNPs | 80/20 | Nanofibers |
| PVA/ HA-AgNPs | 60/40 | Nanofibers |
| PVA/ HA-AgNPs | 50/50 | Nanofibers/beads |
| PVA/ HA-AgNPs | 40/60 | No nanofiber |

**Tab. 2:** Pictures of nanofiber sheets based on different concentration of HA and different ratios of PVA to HA/Ag-NPs

| | 1% HA | 2% HA |
|---|---|---|
| 95:5 | 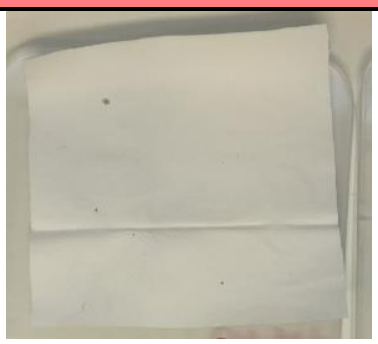 | |
| 90:10 | 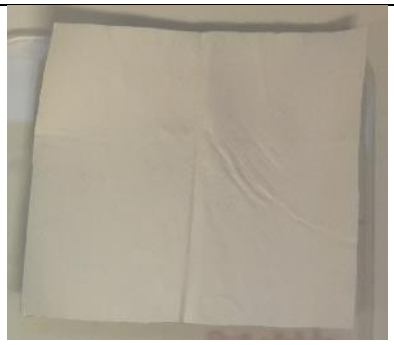 |  |
| 80:20 |  |  |
| 60:40 | 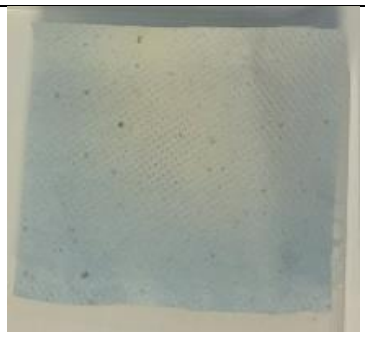 | 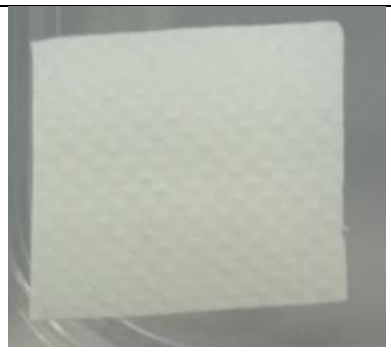 |

| | | |
|---|---|---|
| 50:50 | 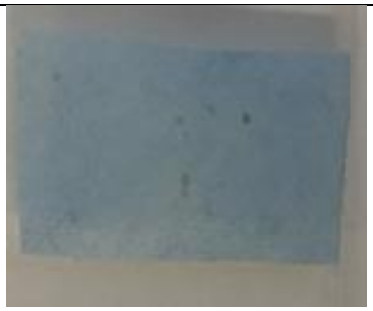 | 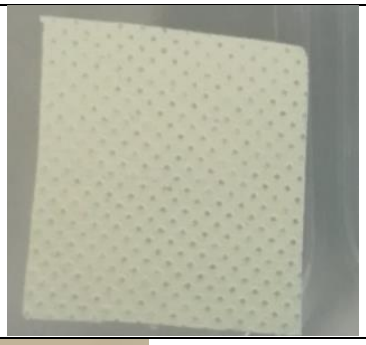 |
| PVA |  | |

In the Tab. 2 are photos of nanofiber sheets prepared from 1 % and 2 % HA, 0.1 M $Ag^{+}$, 20 minutes reaction time blended with PVA in different ratios. Nanofibers were captured on the top of the blue textile carrier. From 16 % PVA it was obtained bright white nanofiber sheet with thickness around 20 µm. Ag-NPs influenced color of nanofiber sheet and with increasing ratio of HA/Ag-NPs nanocomposite in electrospinning solution appeared to have yellowish color of nanofiber sheet. Ratios 95:5; 90:10 and 80:20 acted very similar as PVA solution itself. Preparation of sheets from these ratios was successful and sheets with dimensions around 10 x 10 cm were produced without difficulties. However, processing of samples with lower PVA content was much less straightforward and only very thin layer of nanofibers with small droplets of solution was succeeded to prepare from ratios 60:40 and 50:50. Nanofibers from the solution with the same properties, except 2 % HA instead of 1 %, were not so easy to prepare. It was obtained just small sheets around 4 x 4 cm even after longer time of electrospinning as in the round with 1 % HA.

Fig. 16 shows the proposed schematic mechanism of interaction between PVA and HA/Ag-NPs nanocomposite Due to raised pH of the reaction mixture, the inter/intra hydrogen bonds between the HA chains were destroyed/generated spontaneously. Ag-NPs were interconnected with functional groups of hyaluronan (hydroxyl, carboxyl, acetamide, and partially amino groups) chemically or physically bonded (Fig. 16). Hyaluronan, which was a hydrogen donor, should form hydrogen bonds with the hydroxyl group of PVA. By the incorporation of PVA into HA/Ag-NPs, the probability of hydrogen bonding formation increases (Fig. 16). PVA makes hydrogen bonds between HA and AgNPs in the electrospun nanocomposite (PVA/HA-AgNPs).

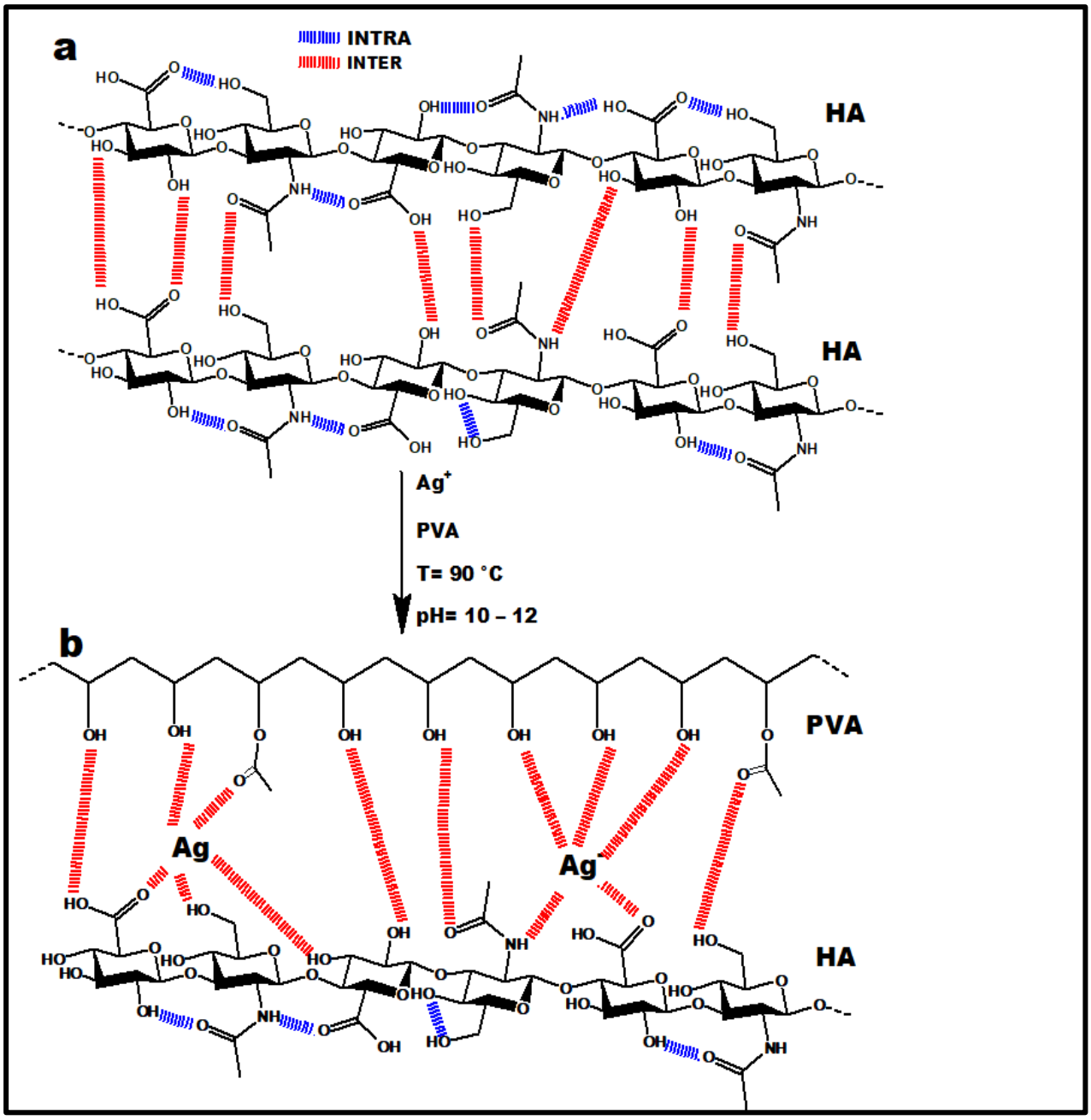


**Fig. 16**: Proposed scheme of interaction between polyvinyl alcohol (PVA) and hyaluronan-silver (HA-AgNPs) nanoparticles composite (PVA/HA-AgNPs)

### 4.6. Morphology of PVA/HA-AgNPS nanofiber mats

Fig. 17 shows SEM micrographs, average diameter, and diameter distribution of the nanofiber mats made of the polyvinyl alcohol (PVA), PVA/HA blend electro spunned nanofibers at different weight ratios of PVA to HA in presence of *in-situ* $Ag^0$. As shown in Fig. 17(a-e), a defect-free nanofibers were observed in mats with net PVA to PVA/ HA Ag-NPs different ratios up to 60/40.

The e-spun fibers in the fiber mats beaded and became irregular in shape at PVA to HA/AgNPs weight ratio 50/50 as can be seen in Fig. 17 f. When the HA content in the PVA/ HA/AgNPs blend was higher than 50 wt %, e-spun fibers could have been just hardly formed. These observations can be explained by the fact that when the concentration of the hyaluronan (a polyanion) in the blend solution increases, the repulsive force between the anionic groups within the polymer's backbone increases. Thus, the formation of continuous fibers is inhibited during the electrospinning process under the high electric field. Simultaneously, as the concentration of hyaluronan in the blend increases from 0 to 20 wt %, the average diameters of PVA/HA blend e-spun fibers decreases from 211 nm to less than 200 nm (Fig. 18 a-c; Fig. 19 a. At the ratio 80/20 distribution become slightly wider and diameter was decreased to 154 nm (Fig. 18 d). This was explained by the effect of hyaluronan which leads to the increased charge density on the surface of the ejected jet formed during electrospinning. By increasing the ratio between HA to PVA (60/40 and 50/50) the diameter distribution become slightly wider again but smaller than net PVA (Fig. 18 e,f; Fig. 19 a). Fig. 19 b shows the distribution of AgNPs onto surface of PVA/HA nanofibers mats without aggregation on the surface on mats.

Due to the very small size of AgNPs (2-5 nm), particles were not visualized using normal SEM. The EDX analysis shows the elemental compositions of PVA, PVA/HA-AgNPs mats with different ration between PVA and HA-AgNPs (80/20;60/40 and 50/50), and the percentage of NPs was increased by increasing the ratio between HA/AgNPs and PVA. At the lower ratio between PVA and HA/Ag-NPs Ag-NPs were not observed, due to the overlapping of NPs by palladium from coating layer.

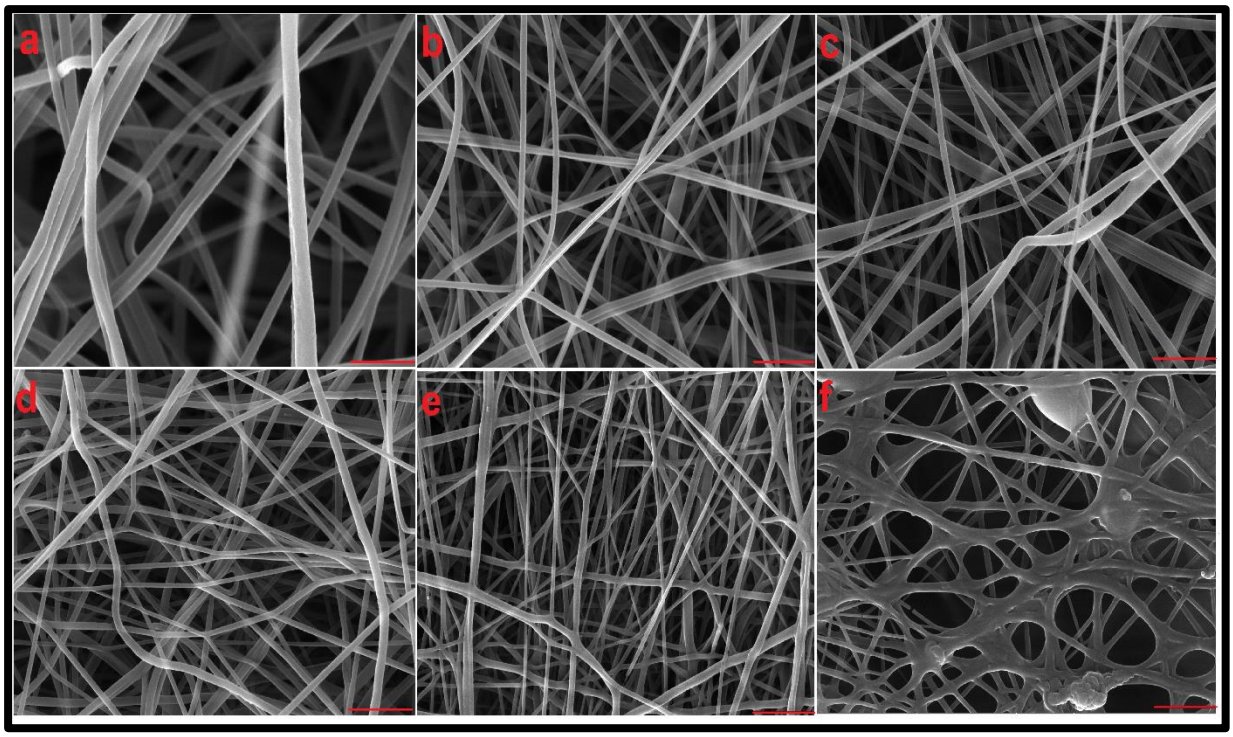


**Fig. 17:** SEM micrographs of e-spun mats fabricated of PVA/HA-AgNPs blend e-spin at different weight ratios between PVA and HA-AgNPs.

**Experimental conditions:** (a) Net PVA; (b) PVA/HA-AgNPs (95/5); (c) PVA/HA-AgNPs (90/10); (d) PVA/HA-AgNPs (80/20); (e) PVA/HA-AgNPs (60/40); (f) PVA/HA-AgNPs (50/50). Scale bars were 2 µm.

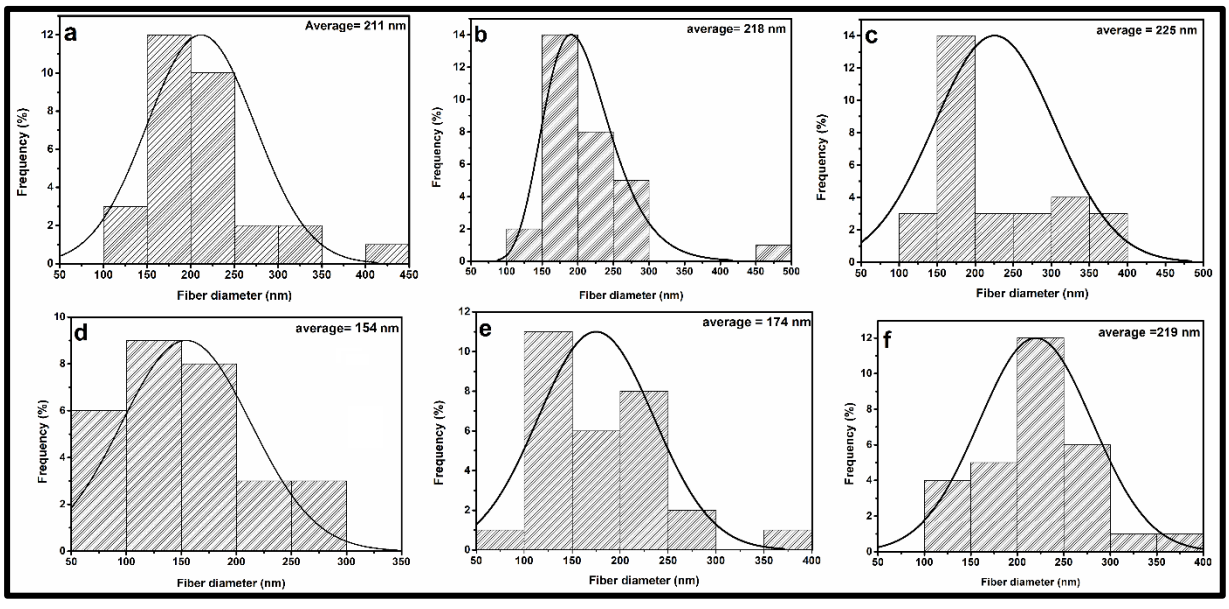


**Fig. 18:** Histogram micrographs of e-spun mats fabricated of PVA/HA-AgNPs blend e-spin at different weight ratios between PVA and HA-AgNPs.

**Experimental conditions:** (a) Net PVA; (b) PVA/HA-AgNPs (95/5); (c) PVA/HA-AgNPs (90/10); (d) PVA/HA-AgNPs (80/20); (e) PVA/HA-AgNPs (60/40); (f) PVA/HA-AgNPs (50/50). Scale bars were 2 µm.

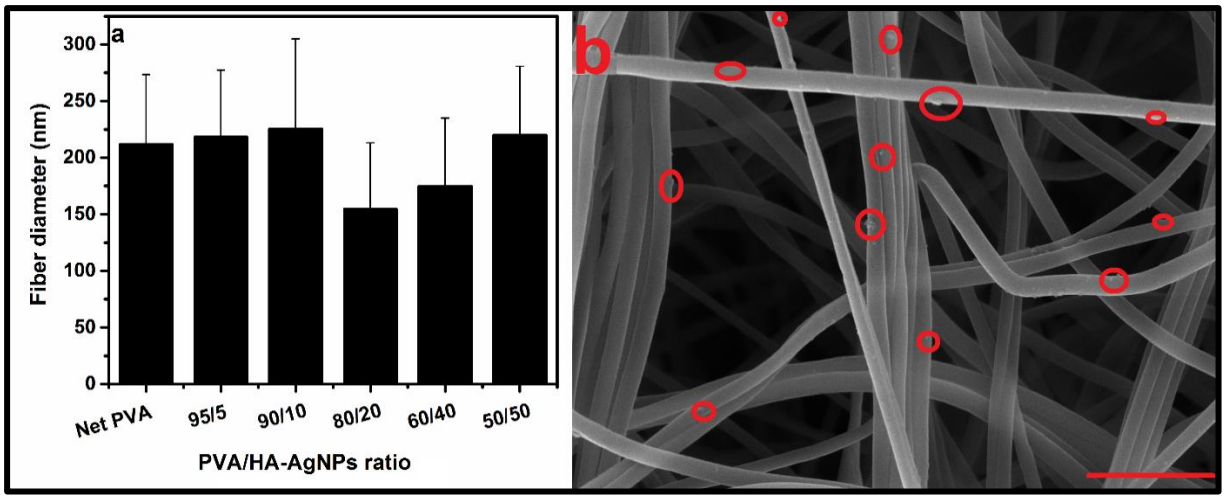


**Fig. 19**: Representation of the different ratios between PVA/HA-AgNPs and fiber diameter and Ag-NPs distribution on the surface of nanofibers (PVA/HA-AgNPs; 50/50)

**Tab. 3:** composition of nanofiber mats fabricated using different ratios.

| *Net PVA* | *Weight (%)* | *PVA/HA-AgNPs (80/20)* | *PVA/HA-AgNPs (60/40)* | *PVA/HA-AgNPs (50/50)* |
|---|---|---|---|---|
| *C* | 58.1 | 42.67 | 46.31 | 29.22 |
| *O* | 41.9 | 47.79 | 46.33 | 49.41 |
| *N* | ------- | 6.63 | 5.40 | 5. 92 |
| *Na* | ----- | 2.83 | 1.67 | 13.92 |
| *Ag* | ------- | 0.08 | 0.29 | 1.54 |

### 3.7. Characterization of nanofiber mats using ATR-FTIR

For characterization of specific chemical groups involved in prepared nanofiber sheets, attenuated total reflectance-Fourier infrared spectroscopy (ATR-FTIR) was used. Obtained absorbance dependent on wavenumber is plotted in Fig. 20 for different ratios of 1 % HA/Ag-NPs: PVA. FTIR spectra for powder HA displays specific band around 3300 $cm^{-1}$ which represents O – H stretching and N – H stretching and could also represents $H_2O$ moieties [49]. Both 2940 $cm^{-1}$ and 2905 $cm^{-1}$ refers to C – H asymmetric stretching of polymer backbone [50]. Further significant groups for HA represent band at 1605 $cm^{-1}$ which refers to C = O stretching of carboxylic group in guluronic acid residues unit of HA [51]. Band at 1315 $cm^{-1}$ could refer to C – OH stretching of carboxylic group. An intense band extending between 950 $cm^{-1}$ and 1200 $cm^{-1}$, corresponds to C – O stretching vibrations in alcohols [52]. The same peak with lower absorbance appeared around 3300 $cm^{-1}$ in PVA nanofiber sheet spectrum referring to hydroxy group. C – H stretching band appeared at 2940 and 2905 $cm^{-1}$, and bending alkane band appeared at 1440 $cm^{-1}$. Stretching band for C = O groups remained from unconverted

polyvinyl acetate into PVA appeared at υ 1720 $cm^{-1}$. Band at 1370 $cm^{-1}$ could be bending of O – H group, and the one at 1250 $cm^{-1}$ could be stretching vibrations of C – O.

Intensity of O – H stretching at 3300 $cm^{-1}$is decreasing, owing to further hydrogen bonding reaction occurred between PVA and HA. Slight broadening of the O – H stretching peak at 3300 $cm^{-1}$ reveals formation of intermolecular hydrogen bonding interactions between the polymers as well [51]. Spectrums of different ratios maintain mostly the shape of PVA absorption spectrum. Band at 1720 $cm^{-1}$ from unconverted polyvinyl acetate could be observed in higher intensities for samples with higher content of PVA in electrospinning solution. Tiny band at 1600 $cm^{-1}$ of C = O stretching increases in intensity with more frequent carbonyl group present in the nanofiber sheet due to higher proportion of HA in electrospinning solution.

Comparable results were attained with ATR-FTIR of nanofiber sheets made of 2% HA/Ag-NPs instead of 1 % HA. Results are available in

Fig. **27** in the section attachments.

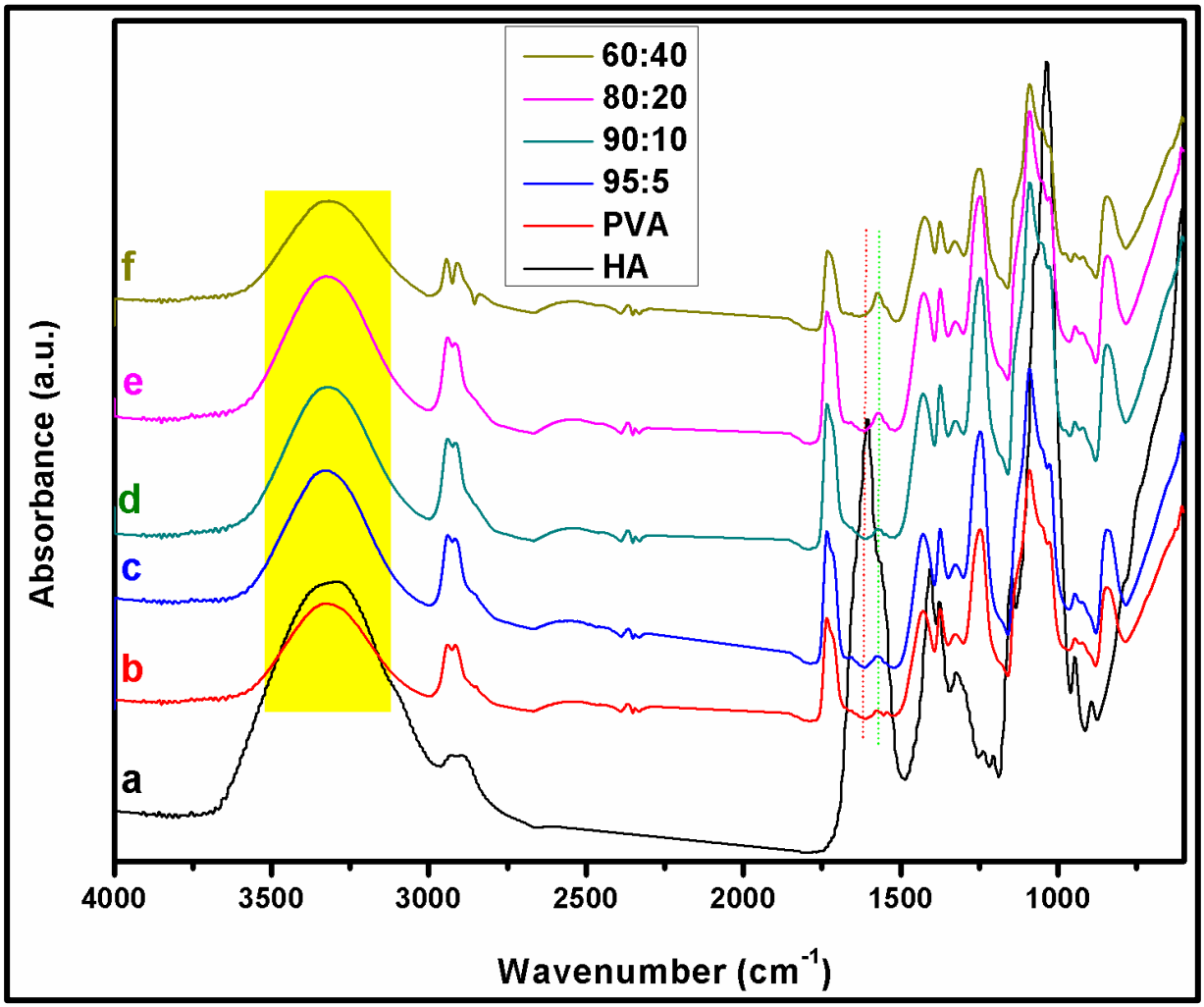


**Fig. 20**: FTIR spectrum of nanofiber sheet made of different ratios of HA/Ag-NPs and PVA

**Experimental conditions**: 1 % HA, 0.1 M Ag+, 1 ml NaOH, 20 min, a) HA powder; b) PVA; c) ratio 95:5; d) ratio 90:10; e) ratio 80:20; f) ratio 60:40

## 3.3 Characterization of thermal stability of electrospun mats

Changes in the thermal stability of pure polymers and their blends were studied under nitrogen flow by thermogravimetric analysis (TGA). The weight loss of the nanofiber films as the function of the temperature are shown in Fig. 21. HA powder, PVA powder, nanofibers from pure PVA and nanofibers of blend of PVA and HA/Ag-NPs were tested.

In Fig. 21 and Fig. 22 are only curves for ratios 90:10 and 60:40 for better intelligibility of figures, but complete figures with all measured variables are available as Fig. 28 and Fig. 29 in attachments. TGA curves in Fig. 21 exhibited weight loss for HA powder, PVA powder, PVA nanofibers and PVA blends nanofibers mostly in 3 stages. First stage is better visible in inset of Fig. 22. First stage is from 30 to 110°C for HA and broader band centered in 120°C for PVA powder is due to loss of moisture and acetyl residuals and it showed approximate 18 %, 5%, 4%, 3%, 3% weight loss, for HA powder, PVA powder, PVA nanofibers and PVA blends nanofibers, respectively. Result indicate that blends entrapped a lower amount of water compared to pure HA and PVA.

The main weight loss for HA occurred between 200°C and 300°C centered at 240°C which was ascribed to partial breakage of molecular structure and weight loss was around 42 % [53].

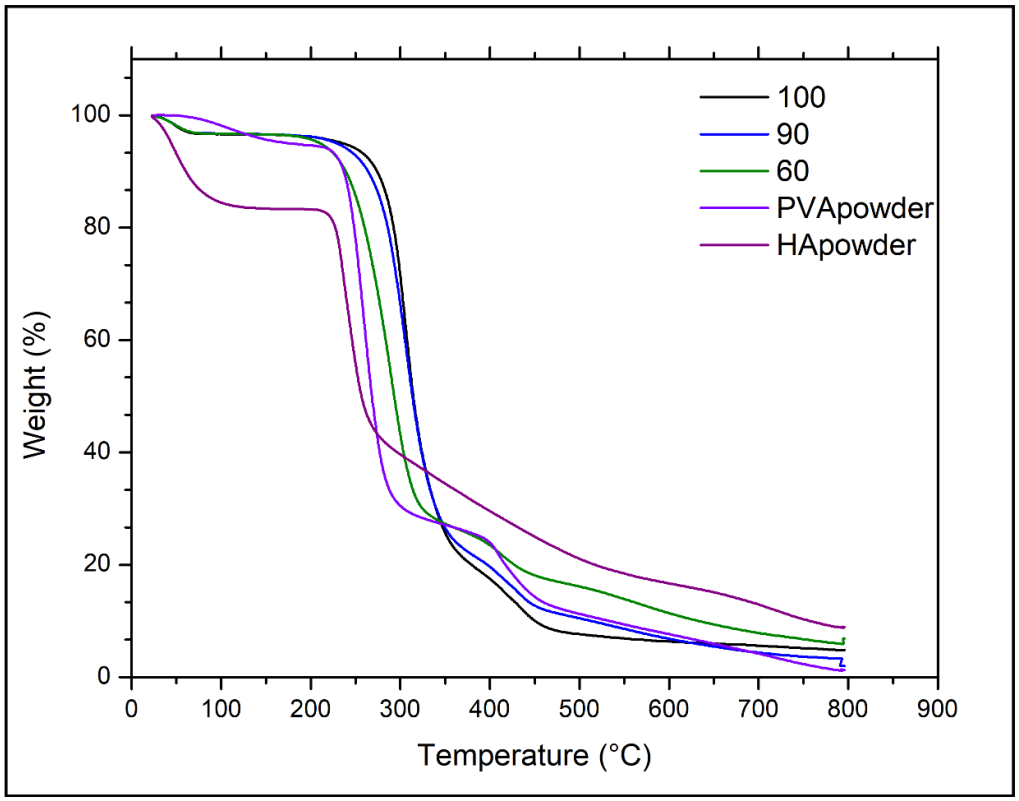


**Fig. 21** TGA curves of 1 % HA/Ag-NPs : PVA nanocomposite and HA powder, PVA powder

**Note:** legend provides percentage content of PVA used for nanocomposite preparation; heating program: 10°C/min to 800°C under nitrogen atmosphere

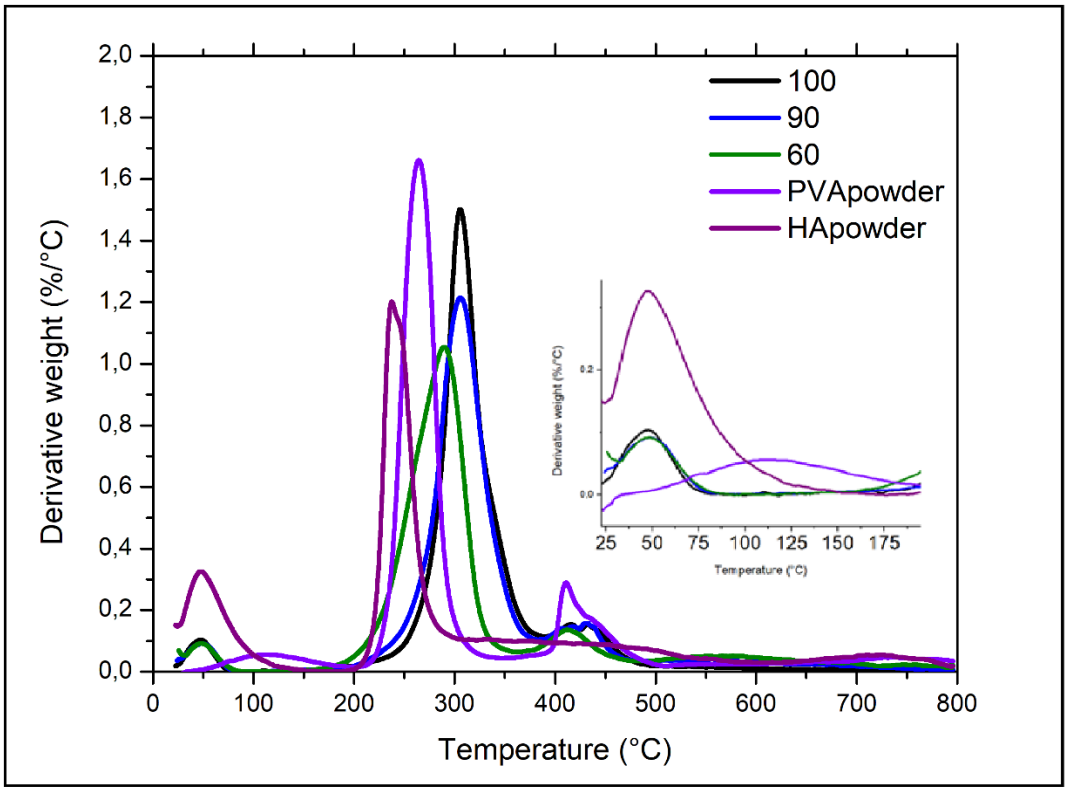


**Fig. 22** DTG curves of 1 % HA/Ag-NPs : PVA nanocomposite and HA powder, PVA powder, detail on weight loss from 25 °C to 175 °C

Note: legend provides percentage content of PVA used for nanocomposite preparation; heating program: 10°C/min to 800°C under nitrogen atmosphere

In the third stage, residues are further degraded with approximately continuous rate of change. In the case of PVA powder, second degradation step takes place at 265 °C related to degradation of amorphous parts of the polymer while third step at 410 °C corresponds to degradation of the higher thermal stable crystalline parts [54]. Peak for derivative thermogravimetric curve in Fig. 22 for PVA fibers and binary blend fibers was shifted to the higher temperatures compared to PVA powder and HA powder concluding higher thermal stability of prepared nanofibers than pure materials.

The addition of HA into the PVA decreases weight loss of PVA nanofibers. PVA nanofibers and binary blend nanofibers showed smaller weight loss in the region from 400 °C to 450 °C compared to PVA powder that could refer to lowering presence of crystalline parts in process of electrospinning. Temperature of decomposition of PVA-HA/Ag-NPs nanocomposite depends on content of PVA and HA, temperature resistance of nanofibers was increased by blending more PVA into electrospinning solution.

Due to good properties for electrospinning, PVA was blended to the HA/Ag-NPs nanocomposite in different ratios. Thermal stability of electrospun nanofibers was improved compared to pure PVA and HA, by blending PVA with HA/Ag-NPs due to hydrogen bonding interactions. Owing to the presence of hydroxyl groups in PVA as well as carboxyl, hydroxyl

and carbonyl group in HA it is possible to combine chains via hydrogen bonds [53]. Similar thermal losses were observed in nanofibers produced from 2 % HA/Ag-NPs and PVA. Results are available in Fig. 30 and Fig. 31 in attachments.

### 3.4 XRD of wound dressing mats

Fig. 23 shows the X-ray diffraction of the wound dressing mats fabricated using different weight ratios between PVA and HA/Ag-NPs nanocomposite using (1 % HA). Net PVA show only broad reflection peak $2\theta = 20^0$, due to semi-crystalline property of the PVA. Moreover, the XRD peaks for the AgNPs are found at 38.2°, 44.6° 64.6° and 78.9° of 2θ, which are indexed to the (111) (200), (220), and (311) planes with cubic symmetry, respectively. This confirmed that the fabricated AgNPs crystals were stabilized using HA in these samples due to the existence of HA/PVA molecules, even just very small ones. The intensity of the AgNPs peaks were increased by increasing the ratio between PVA and HA-AgNPs. However, the peaks of the silver nanocrystals from the PVA/ HA/Ag-NPs mats, which contains the lowest content of AgNPs (95/5 and 90/10 weight ratio), could hardly been detected due to the resolution limit of XRD analysis.

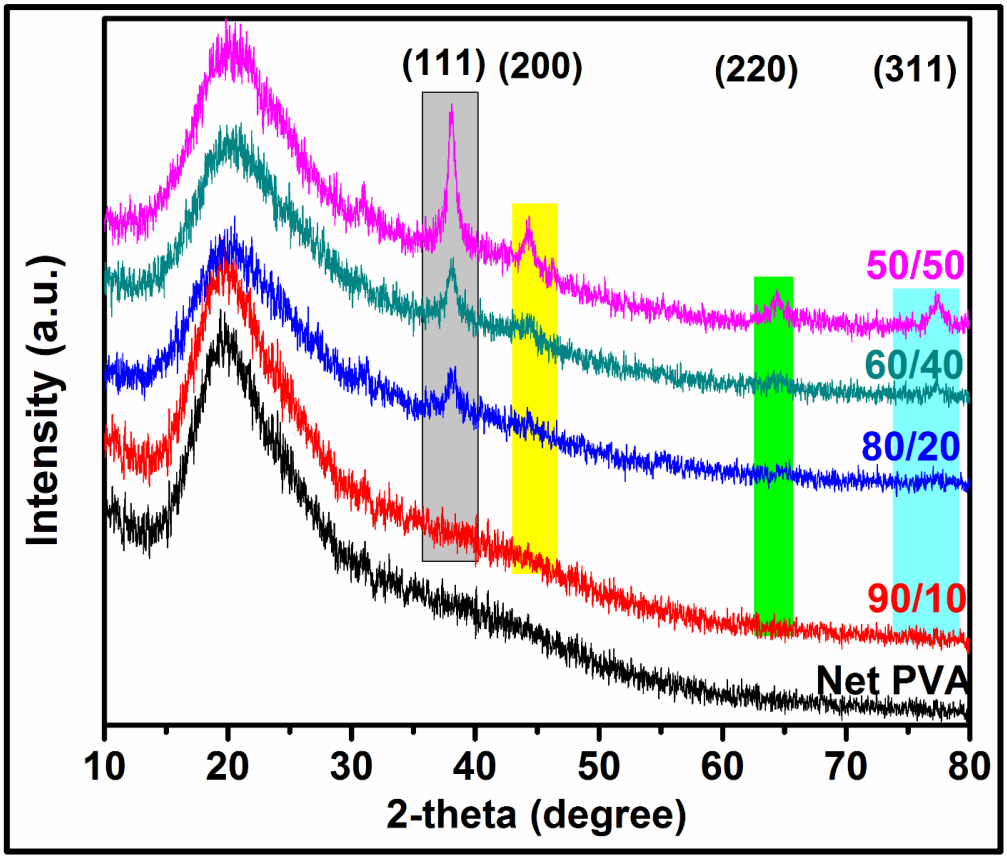


**Fig. 23:** XRD of wound dressing mats with different ratio between PVA and HA/Ag-NPs

**Experimental conditions**: 1 % HA, 0.1 M Ag+, 1 ml NaOH, 20 min, and different ratio between nanofibers mats compositions (Net PVA, PVA/HA-NPs (90/10); PVA/HA-NPs (80/20); PVA/HA-NPs (60/40); PVA/HA-NPs (50/50).

## 3.5 Mechanical properties of wound dressing mats

Characterization continued with tensile testing of prepared nanofibers. Possibility of testing ratios with higher content of HA (50:50; 60:40) was reduced due to obtaining just small sheets of nanofibers. Around 15 samples from each ratio possible to test (PVA sheet, ratios 95:5; 90:10; 80:20) were studied and average curves of stress-strain dependence are provided in the Fig. 24 and Fig. 25.

It can be observed quite linear dependence for PVA nanofibers with stress at break around 3.5 MPa from Fig. 24. Sheets composed of bled of PVA and HA/Ag-NPs exhibited higher stress at break, approximately 5,2 MPa, 6.2 MPa, and 8,2 MPa for ratios 95:5, 90:10, 80:20, respectively. Higher tensile strength of binary blends nanofibers could be caused by new interactions between PVA and HA. In Fig. 25 are stress-strain curves of nanofibers made from PVA and 2 % HA which differs in shape from fibers prepared from 1 % HA. However, stress at break is approximately 3.5 MPa, 4.5 MPa and 6.5 MPa for PVA and ratios 90:10 and 80:20, respectively. Trend of increasing nanofiber sheet´s strength at break resembles previous samples made of 1 % HA. From this can be conclude that optimal ratio according to handling and manipulation with wound dressing is 80:20, and ratio 80:20 based on 1 % HA reached even higher value of strength at break than sample 80:20 based on 2 % HA.

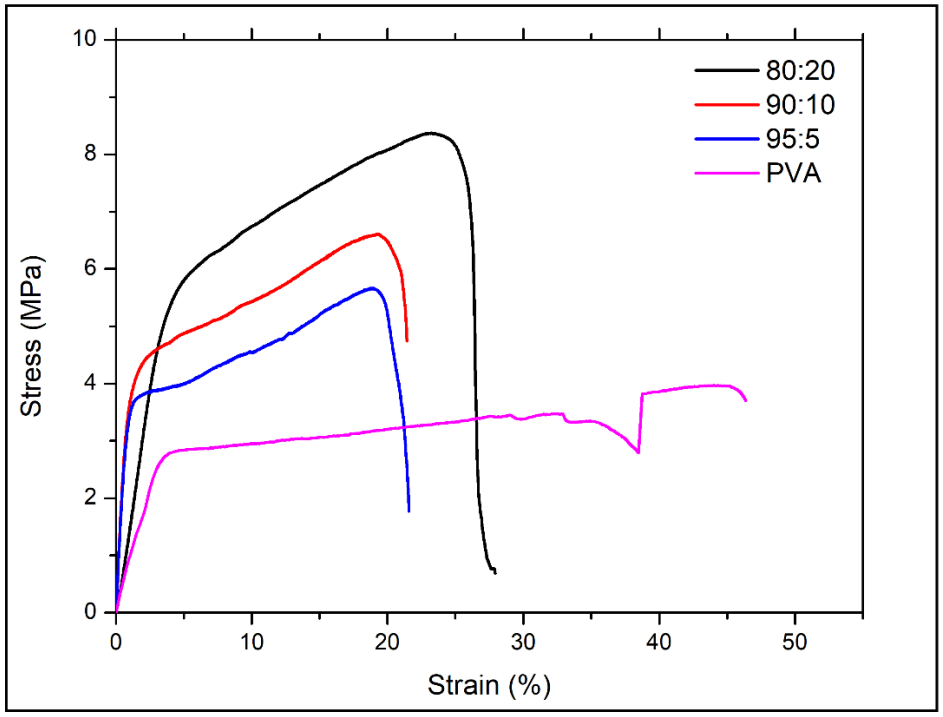


**Fig. 24:** Stress-strain curve of nanofiber sheet made of different ratios of 1 % HA/Ag-NPs and PVA.

Tab. 4 shows average E-modulus and Stress at break of more measured samples, suggest the same trend as it was observed in stress-strain curves. Both E-modulus and stress at break are increasing with increasing content of HA/Ag-NPs in preparation solution proposing ratio 80/20 as the best one in order to mechanical properties.

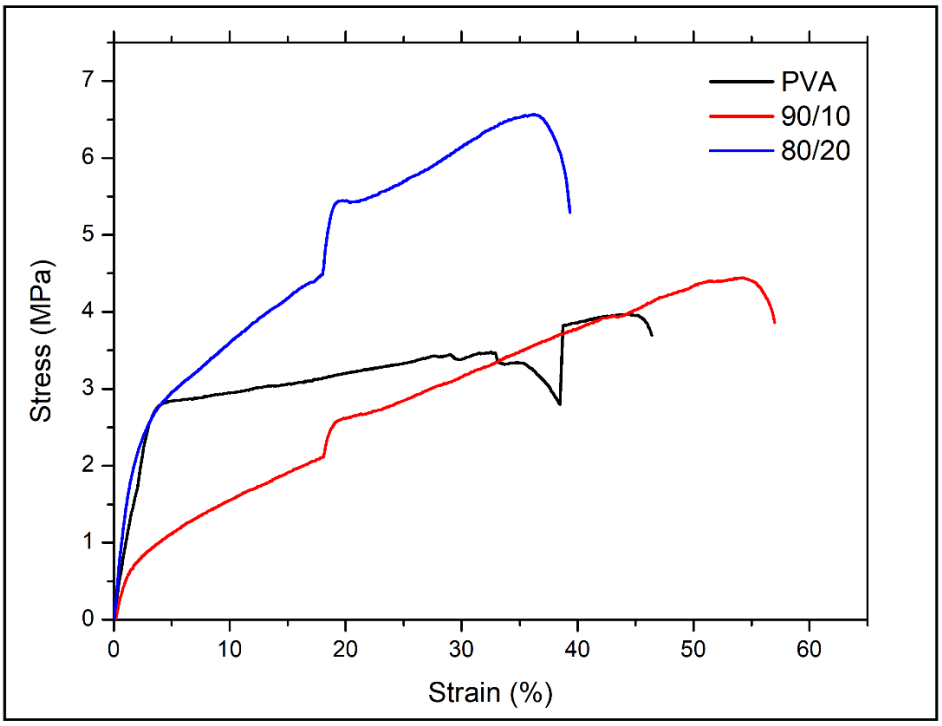


**Fig. 25:** Stress-strain curve of nanofiber sheet made of different ratios of 2 % HA/Ag-NPs and PVA.

**Tab. 4:** Average values of E-Modulus and Stress at break of sheets prepared by different ratio of HA/Ag-NPs: PVA; (1 % HA and 2 % HA tested).

| E-modulus (MPa) | | | |
|---|---|---|---|
| | | | |
| 1 % HA | | 2% HA | |
| 95/5 | 244.9 | 95/5 | |
| 90/10 | 339.6 | 90/10 | 58.8 |
| 80/20 | 315.0 | 80/20 | 118.5 |
| PVA 16 % | 185.1 | | |
| **Stress at break (MPa)** | | | |
| 1 % HA | | 2 % HA | |
| 95/5 | 3.2 | 95/5 | |
| 90/10 | 3.4 | 90/10 | 3.2 |
| 80/20 | 4.5 | 80/20 | 4.4 |
| PVA 16 % | 3.0 | | |

# 4. CONCLUSION

Good integration of materials into biologically relevant systems and eco – friendliness of wound dressings prepared by "green-way" was the main inspiration for preparing a new wound dressing based on hyaluronan/silver nanoparticles. *In-situ* prepared Ag-NPs in HA/Ag-NPs nanocomposite were both reduced and stabilized by high molecular weight hyaluronic acid and no toxic external reducing agents such as hydrazine hydrate [55], N,N-dimethyl formamide [56], or sodium borohydrate [57], were used.

Optimal parameters for nanocomposite synthesis was reducing 0.1 M $AgNO_3$ by 1 % HA with molecular weigh 1.7 MDa at basic conditions and temperature 90 °C. Presence of Ag-NPs in nanocomposite was demonstrated by UV/Vis absorption at approximately 410 nm and their average size was discovered to be in range from 2 nm to 6 nm with negligible changes in size of NPs with different time of reactions, according to DLS and TEM.

Wound dressing nanofiber sheets were prepared by electrospinning process from rotating string electrode at voltage 58 kV and electrospun solution consisted of different ratios of PVA and previously prepared HA/Ag-NPs nanocomposite. Viscosity of different ratios of electrospun solutions showed increasing trend with increased content of PVA in the solution. Prepared mats were studied by SEM and nanofiber character of sheets was confirmed. According to workability of electroospun solution by electrospinning machine and, later studied shape of nanofibers, the best ratios for electrospinning are from 100 % PVA down to the ratio 80:20 between PVA and HA/Ag-NPs, respectively. EDX analysis confirmed presence of Ag in small amount in samples with higher contents of HA/Ag-NPs (50:50; 60:40). Further ATR-FTIR analysis proved the presence of groups of HA and PVA and suggests formation of hydrogen bonds between HA and PVA as it was proposed on the scheme in the discussion. TGA revealed findings of higher temperature stability of PVA/Ag-NPs nanofibers comparing to pure HA and PVA what also propose to think about formation of the new bonds between HA and PVA. According to the importance of convenient manipulation at wound dressing applications, tensile testing was carried out. Strength dependence on PVA:HA/Ag-NPs ratio presented ratio 80:20 to be the strongest one.

With these findings, study covered revealing of the optimal preparation conditions on HA/Ag-NPs wound dressing. Next goal could be the use of this wound dressing as a drug carrier and further toxicity tests.

## 4.1 Graphical conclusion

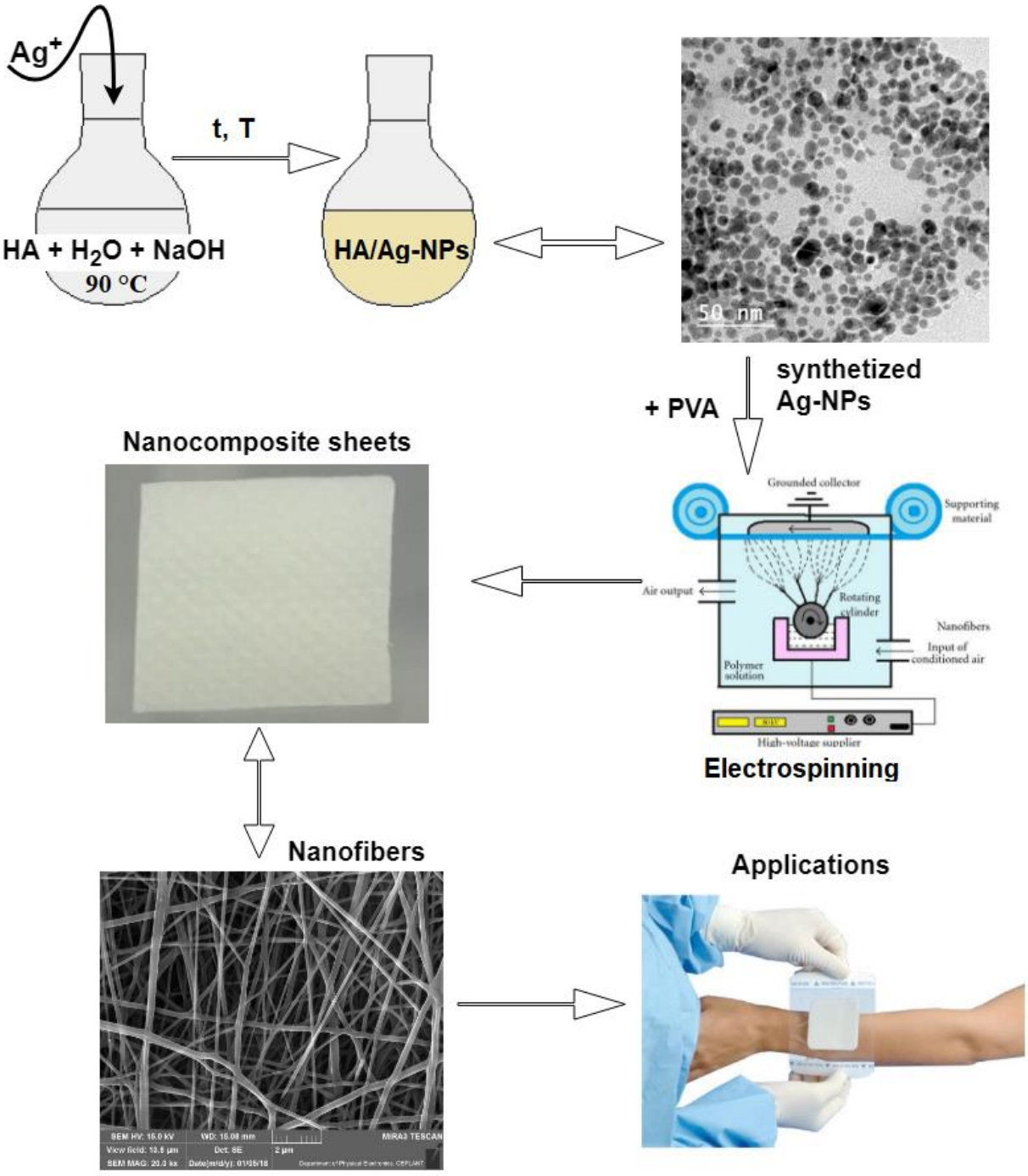


**Fig. 26** Scheme of steps of HA/Ag-NPs wound dressing preparation.

## REFERENCES


[1] DHIVYA, Selvaraj, Viswanadha PADMA a Elango SANTHINI. *Wound dressings – a review*. b.r. DOI: 10.7603/s40681-015-0022-9. Available from: http://www.globalsciencejournals.com/article/10.7603/s40681-015-0022-9

[2] DEGREEF, Hugo. HOW TO HEAL A WOUND FAST. *Dermatologic Clinics*. 1998, 16(2), 365-375. DOI: 10.1016/S0733-8635(05)70019-X. ISSN 07338635. Available from: http://linkinghub.elsevier.com/retrieve/pii/S073386350570019X

[3] TARNUZZER, Roy a Gregory SCHULTZ. *Biochemical analysis of acute and chronic wound environments*. b.r. DOI: 10.1046/j.1524-475X.1996.40307.x. Available from: http://doi.wiley.com/10.1046/j.1524-475X.1996.40307.x

[4] SHAH, Jayesh. The History of Wound Care. *The Journal of the American College of Certified Wound Specialists*. 2011, 3(3), 65-66. DOI: 10.1016/j.jcws.2012.04.002. ISSN 18764983. Available from: http://linkinghub.elsevier.com/retrieve/pii/S1876498312000069

[5] BOATENG, Joshua, Kerr MATTHEWS, Howard STEVENS a Gillian ECCLESTON. Wound Healing Dressings and Drug Delivery Systems: A Review. *Journal of Pharmaceutical Sciences*. 2008, 97(8), 2892-2923. DOI: 10.1002/jps.21210. ISSN 00223549. Available from: http://linkinghub.elsevier.com/retrieve/pii/S0022354916326521

[6] SIMõES, Déborah, Sónia MIGUEL, Maximiano RIBEIRO, Paula COUTINHO, António MENDONçA a Ilídio CORREIA. Recent advances on antimicrobial wound dressing: A review. *European Journal of Pharmaceutics and Biopharmaceutics*. 2018, **127,** 130-141. DOI: 10.1016/j.ejpb.2018.02.022. ISSN 09396411. Available from: http://linkinghub.elsevier.com/retrieve/pii/S0939641117315023

[7] WANG, Lishan, Eugene KHOR, Aileen WEE a Lee Yong LIM. Chitosan-alginate PEC membrane as a wound dressing: Assessment of incisional wound healing. *Journal of Biomedical Materials Research*. 2002, 63(5), 610-618. DOI: 10.1002/jbm.10382. ISSN 0021-9304. Available from: http://doi.wiley.com/10.1002/jbm.10382

[8] JOLLY, S. Dry wound healing concept using spray-on dressings for chronic wounds. *Advanced Wound Repair Therapies*. Elsevier, 2011, , 209-226. DOI: 10.1533/9780857093301.2.209. ISBN 9781845697006. Available from: http://linkinghub.elsevier.com/retrieve/pii/B9781845697006500085

[9] SARABAHI, Sujata. Recent advances in topical wound care. *Indian Journal of Plastic Surgery*. 2012, 45(2), 379-. DOI: 10.4103/0970-0358.101321. ISSN 0970-0358. Available from: http://www.ijps.org/text.asp?2012/45/2/379/101321

[10] SOOD, Aditya, Mark GRANICK a Nancy TOMASELLI. Wound Dressings and Comparative Effectiveness Data. *Advances in Wound Care*. 2014, **3**(8), 511-529. DOI:

10.1089/wound.2012.0401. ISSN 2162-1918. Available from: http://online.liebertpub.com/doi/abs/10.1089/wound.2012.0401

[11] O'BRIEN, Fergal. Biomaterials & scaffolds for tissue engineering. *Materials Today*. 2011, 14(3), 88-95. DOI: 10.1016/S1369-7021(11)70058-X. ISSN 13697021. Available from: http://linkinghub.elsevier.com/retrieve/pii/S136970211170058X

[12] MOHANDAS, Annapoorna, S. DEEPTHI, Raja BISWAS a R. JAYAKUMAR. Chitosan based metallic nanocomposite scaffolds as antimicrobial wound dressings. *Bioactive Materials*. 2018, 3(3), 267-277. DOI: 10.1016/j.bioactmat.2017.11.003. ISSN 2452199X. Available from: http://linkinghub.elsevier.com/retrieve/pii/S2452199X17300166

[13] WU, Jian, Yudong ZHENG, Wenhui SONG et al. In situ synthesis of silver-nanoparticles/bacterial cellulose composites for slow-released antimicrobial wound dressing. *European Journal of Pharmaceutics and Biopharmaceutics*. 2018, (127), 130-141. DOI: 10.1016/j.carbpol.2013.10.093. Available from: http://linkinghub.elsevier.com/retrieve/pii/S0144861713011223

[14] AUGUSTINE, Robin, Nandakumar KALARIKKAL a Sabu THOMAS. Electrospun PCL membranes incorporated with biosynthesized silver nanoparticles as antibacterial wound dressings. *Applied Nanoscience*. 2016, **6**(3), 337-344. DOI: 10.1007/s13204-015-0439-1. ISSN 2190-5509. Available from: http://link.springer.com/10.1007/s13204-015-0439-1

[15] ABDEL-MOHSEN, A.M., J. JANCAR, R.M. ABDEL-RAHMAN, L. VOJTEK, P. HYRŠL, M. DUŠKOVÁ a H. NEJEZCHLEBOVÁ. A novel in situ silver/*hyaluronan bio-nanocomposite fabrics for wound* and chronic ulcer dressing: In vitro and in vivo evaluations. International Journal of Pharmaceutics. 2017, 520(1-2), 241-253. DOI: 10.1016/j.ijpharm.2017.02.003. ISSN 03785173. Available from: http://linkinghub.elsevier.com/retrieve/pii/S0378517317300844

[16] ANISHA, B.S., Raja *BISWAS, K.P. CHENNAZHI a R. JAYAKUMAR*. Chitosan–hyaluronic acid/nano silver composite sponges for drug resistant bacteria infected diabetic wounds. *International Journal of Biological Macromolecules*. 2013, 62, 310-320. DOI: 10.1016/j.ijbiomac.2013.09.011. ISSN 01418130. Available from: http://linkinghub.elsevier.com/retrieve/pii/S0141813013004844

[17] THOMAS E. TWARDOWSKI., . Introduction to *nanocomposite materials: properties, processing*, characterization. Lancaster, Pa: Destech Publications, Inc, 2007. ISBN 978-193-2078-541.

[18] VOLLATH, D. a Manasa. MEDIKONDA. Nanoparticles--nanocomposites--nanomaterials: an introduction for *beginners.* Weinheim, Germany: Wiley-VCH, 2013. ISBN 978-3-527-67071-0.

[19] BOGUE, Robert. Nanocomposites: a review of technology and applications. Assembly Automation. 2011, 31(2), 106-112. DOI: 10.1108/01445151111117683. ISSN 0144-5154. Available from: https://www.emeraldinsight.com/doi/10.1108/01445151111117683

[20] Nanocomposites – An Overview of Properties, Applications and Definition. Azonano [online]. 2007 [cit. 2018-04-01]. Dostupné z: https://www.azonano.com/article.aspx?ArticleID=1832

[21] LEPCIO, Petr, Frantisek ONDREAS, Klara ZARYBNICKA, Marek ZBONCAK, Ondrej CAHA a Josef JANCAR. Bulk polymer nanocomposites with preparation protocol governed nanostructure: the origin and properties of aggregates and polymer bound clusters. *Soft Matter*. 2018, 14(11), 2094-2103. DOI: 10.1039/C8SM00150B. ISSN 1744-683X. Available from: http://xlink.rsc.org/?DOI=C8SM00150B

[22] Nanocomposites, their Uses *and Applications. Understandingnano* [online]. Hawk's Perch Technical Writing, 2016 [cit. 2018-04-01]. Dostupné z: http://www.understandingnano.com/nanocomposites-applications.html

[23] SCHWAB, M. Encyclopedic reference of cancer. New York: Springer, 2001. ISBN 978-354-0665-274.

[24] KHABAROV, V., P. BOYKOV a M. SELYANIN. *Hyaluronic acid: preparation, properties, application in biology and medicine*. Chichester, West Sussex, 2015. ISBN ISBN:978-1-118-63379-3.

[25] *FOUDA, Moustafa, A.M.* ABDEL-MOHSEN, Hossam EBAID et al. Wound healing of different molecular weight of hyaluronan; in-vivo study. International Journal of Biological Macromolecules. 2016, 89, 582-591. DOI: 10.1016/j.ijbiomac.2016.05.021. ISSN 01418130. Available from: http://linkinghub.elsevier.com/retrieve/pii/S0141813016304329

[26] KUNDRÁT, Vojtěch. *PŘÍPRAVA NANOVLÁKEN POMOCÍ ELEKTROSTATICKÉHO ZVLÁKŇOVÁNÍ. Brno, 2016*. Master´s thesis. MASARYKOVA UNIVERZITA.

[27] JEDNODUCHÉ TEORETICKÉ ÚVAHY KE ZVLÁKŇOVÁNÍ NANOVLÁKEN [online]. 2009, , *16 [cit. 2018-04-04]*. Dostupné z: http://konsys-t.tanger.cz/files/proceedings/nanocon_09/Lists/Papers/115.pdf

[28] DIVÍNOVÁ, Nikol. Reologické chování roztoků polymeru vhodných pro *elektrostatické zvlákňování.* Brno, 2017. Master´s thesis. Vysoké učení technické v Brne , Fakulta Chemická.

[29] FRENOT, Audrey a Ioannis CHRONAKIS. Polymer *nanofibers assembled by electrospinning. 2003, 8(*1), 64-75. DOI: 10.1016/S1359-0294(03)00004-9. ISSN 13590294. Available from: http://linkinghub.elsevier.com/retrieve/pii/S1359029403000049

[30] RÄTY, Jukka, K. PEIPONEN *a Toshimitsu ASAKURA. UV-visible reflection* spectroscopy of liquids. New York: Springer, 2004. Springer series in optical sciences, v. 92. ISBN 35-404-0582-8.

[31] TISSUE, Brian. Ultraviolet and Visible Absorption Spectroscopy. Characterization of Materials. Hoboken, NJ, USA, 2002. DOI: 10.*1002/0471266965*.com059. ISBN 0471266965. Available from: http://doi.wiley.com/10.1002/0471266965.com059

[32] KUMAR, C. a Hao. JING. UV-VIS and photoluminescence spectroscopy for nanomaterials characterization. New York: Springer Reference, 2013. Springer reference. ISBN 978-3-642-27593-7.

[33] GORBENKO, Galyna a *Valeriya TRUSOVA. Protein aggregation in a membrane* environment. Elsevier, 2011, , 113-142. Advances in Protein Chemistry and Structural Biology. DOI: 10.1016/B978-0-12-386483-3.00002-1. ISBN 9780123864833. Available from: http://linkinghub.elsevier.com/retrieve/pii/B9780123864833000021

[34] STETEFELD, Jörg, Sean MCKENNA a Trushar PATEL. Dynamic light scattering: a practical guide and applications in biomedical sciences. Biophysical Reviews. 2016, 8(4), 409-427. DOI: 10.1007/s12551-016-0218-6. ISSN 1867-2450. Available from: http://link.springer.com/10.1007/s12551-016-0218-6

[35] Dynamic light scattering. Wikiwand [online*]*. b.r. [cit. 2018-05-11]. Dostupné z: http://www.wikiwand.com/en/Dynamic_light_scattering

[36] DIVÍNOVÁ, Nikol. REOLOGICKÉ CHOVÁNÍ ROZTOKŮ POLYMERU VHODNÝCH PRO ELEKTROSTATICKÉ ZVLÁKŇOVÁNÍ. Brno, 2017. Master´s thesis. *Brno University* of Technology.

[37] Scanning electron *microscope. Britannica* [online]. 2018 [cit. 2018-05-11]. Dostupné z: https://www.britannica.com/technology/scanning-electron-microscope

[38] Scanning Electron Microscopy (SEM). Carleton [online]. *b.r. [cit. 2018-05-11]. Dostupné* z: https://serc.carleton.edu/research_education/geochemsheets/techniques/SEM.html

[39] GUNNING, William a Edward CALOMENI. *A* Brief Review of Transmission Electron Microscopy and Applications in Pathology. Journal of Histotechnology. 2013, 23(3), 237-246. DOI: 10.1179/his.2000.23.3.237. ISSN 0147-8885. Available from: http://www.tandfonline.com/doi/full/10.1179/his.2000.23.3.237

[40] Transmission-electron-microscopy. Cmrf.research.uiowa [online]. *b.r. [cit. 2018-05-11]*. Dostupné z: https://cmrf.research.uiowa.edu/transmission-electron-microscopy

[41] DAVID B. WILLIAMS, a C. BARRY CARTER. Transmission electron microscopy a textbook for materials science [online]. 2nd ed. New York: Springer, 2009 [cit. 2018-05-11]. ISBN 978-038-7765-013.

[42] How an FTIR Spectrometer Operates. Chem.libretexts [online]. California: MindTouch®, 2015 [cit. 2018-05-11]. Dostupné *z: https:*//chem.libretexts.org/Core/Physical_and_Theoretical_Chemistry/Spectroscopy/Vibrational_Spectroscopy/Infrared_Spectroscopy/How_an_FTIR_Spectrometer_Operates

[43] ALVAREZ-ORDÕNEZ, Avelino. a Miguel. PRIETO. Fourier transform infrared spectroscopy in food microbiology. New York: Springer, 2012. SpringerBriefs in food, health, and nutrition. ISBN 978-1-4614-3812-0.

[44] Contributions-of-michelson-interferometer-to-ft-ir-spectroscopy. Lab-training [online]. b.r. [cit. 2018-05-11]. Dostupné z: http://lab-training.com/2015/05/08/contributions-of-michelson-interferometer-to-ft-ir-spectroscopy/

[45] DUNN, J.G. a Xuân PHạM. Thermogravimetric Analysis: the origin, *evolution,* and impact of doi moi. Characterization of Materials. Hoboken, NJ, USA, 2002. DOI: 10.1002/0471266965.com029. ISBN 0471266965. Available from: http://doi.wiley.com/10.1002/0471266965.com029

[46] XRD. Serc.carleton [online]. Michigan University, b.r. [cit. *2018-05-13]*. Dostupné z: https://serc.carleton.edu/research_education/geochemsheets/techniques/XRD.html

[47] ABDEL-MOHSEN, A.M., Radim HRDINA, Ladislav BURGERT et al. Antibacterial *activity and* cell viability of hyaluronan fiber with silver nanoparticles. Carbohydrate Polymers. 2013, 92(2), 1177-1187. *DOI:* 10.1016/j.carbpol.2012.08.098. ISSN 01448617. Available from: http://linkinghub.elsevier.com/retrieve/pii/S0144861712008892

8] ABDEL-MOHSEN, A.M., Radim HRDINA, Ladislav BURGERT, Gabriela KRYLOVÁ, Rasha *ABDEL-RAHMAN,* Anna KREJČOVÁ**,** Miloš STEINHART a Ludvík BENEŠ. Green synthesis of hyaluronan fibers with silver nanoparticles. *Carbohydrate Polymers*. 2012, 89(2), 411-422. DOI: 10.1016/j.carbpol.2012.03.022. ISSN 01448617. Available from: http://linkinghub.elsevier.com/retrieve/pii/S0144861712002342

[49] Hydration of Polysaccharide Hyaluronan Observed by IR Spectrometry. I. Preliminary Experiments and *Band* Assignments. Biopolymers (Biospectroscopy). 2003, 2003(72), 11.

[50] BHATTACHARYA, Priyanka, Nathan CONROY, Apparao RAO, Brian POWELL, David LADNER *a Pu* KE. PAMAM dendrimer for mitigating humic foulant. RSC Advances. 2012, 2(21), 7997-. DOI: 10.1039/c2ra21245e. ISSN 2046-2069. Available from: http://xlink.rsc.org/?DOI=c2ra21245e

[51] Ion Conducting Nanocomposite Membranes Based on PVA-HA-HAP for Fuel Cell Application: II. *Effect* of Modifier Agent of PVA on Membrane Properties. Electrockemical Science. 2015, 2015(10), 18.

[52] Infrared Spectroscopy Absorption Table. Chem libretexts [online]. The California State University *Affordable* Learning Solutions: MindTouch®, 2014 [cit. 2018-05-07]. Dostupné z: https://chem.libretexts.org/Reference/Reference_Tables/Spectroscopic_Parameters/Infrared_Spectroscopy_Absorption_Table

[53] LEWANDOWSKA, Katarzyna, Alina SIONKOWSKA, Sylwia GRABSKA a Beata KACZMAREK. Surface and *thermal* properties of collagen/hyaluronic acid blends containing chitosan. International Journal of Biological Macromolecules. 2016, 92, 371-376. DOI: 10.1016/j.ijbiomac.2016.07.055. ISSN 01418130. Available from: http://linkinghub.elsevier.com/retrieve/pii/S0141813016308790

[54] DASSIOS, Konstantinos. Poly(Vinyl Alcohol)-Infiltrated Carbon Nanotube Carpets. Materials Sciences *and Applications*. 2012, 03(09), 658-663. DOI: 10.4236/msa.2012.39096. ISSN 2153-117X. Available from: http://www.scirp.org/journal/doi.aspx?DOI=10.4236/msa.2012.39096

[55] TATARCHUK, Vladimir V., Anastasiya P. SERGIEVSKAYA, Tamara M. KORDA, *Irina A*. DRUZHININA a Vladimir I. ZAIKOVSKY. Kinetic Factors in the Synthesis of Silver Nanoparticles by Reduction of Ag with Hydrazine in Reverse Micelles of Triton N-42. Chemistry of Materials. 2013, 25(18), 3570-3579. DOI: 10.1021/cm304115j. ISSN 0897-4756. Available from: http://pubs.acs.org/doi/10.1021/cm304115j

[56] PASTORIZA-SANTOS, Isabel a Luis LIZ-MARZÁN. Synthesis of Silver Nanoprisms in DMF. *Nano Letters*. 2002, 2(8), 903-905. DOI: 10.1021/nl025638i. ISSN 1530-6984. Available from: http://pubs.acs.org/doi/abs/10.1021/nl025638i

[57] VAN HYNING, Dirk a Charles ZUKOSKI. Formation Mechanisms and Aggregation Behavior of *Borohydride* Reduced Silver Particles. Langmuir. 1998, 14(24), 7034-7046. DOI: 10.1021/la980325h. ISSN 0743-7463. Available from: http://pubs.acs.org/doi/abs/10.1021/la980325h

# 5. LIST OF ABBREVIATIONS

| | |
|---|---|
| c | molar concentration |
| DLS | Dynamic Light Scattering |
| EDX | Energy-dispersive X-ray spectroscopy |
| FTIR | Fourier-Transformed Infrared spectroscopy |
| HA | hyaluronic acid |
| MW | molecular weight |
| NPs | nanoparticles |
| NaOH | sodium hydroxide |
| PVA | polyvinyl alcohol |
| SEM | Scanning Electron Microscopy |
| TEM | Transmission Electron Microscopy |
| TGA | Thermogravimetry Analysis |
| UV/Vis | Ultra Violet/ Visible spectroscopy |
| XRD | X-Ray Diffraction |

# 6. LIST OF ATTACHMENTS

# 7. ATTACHMENTS

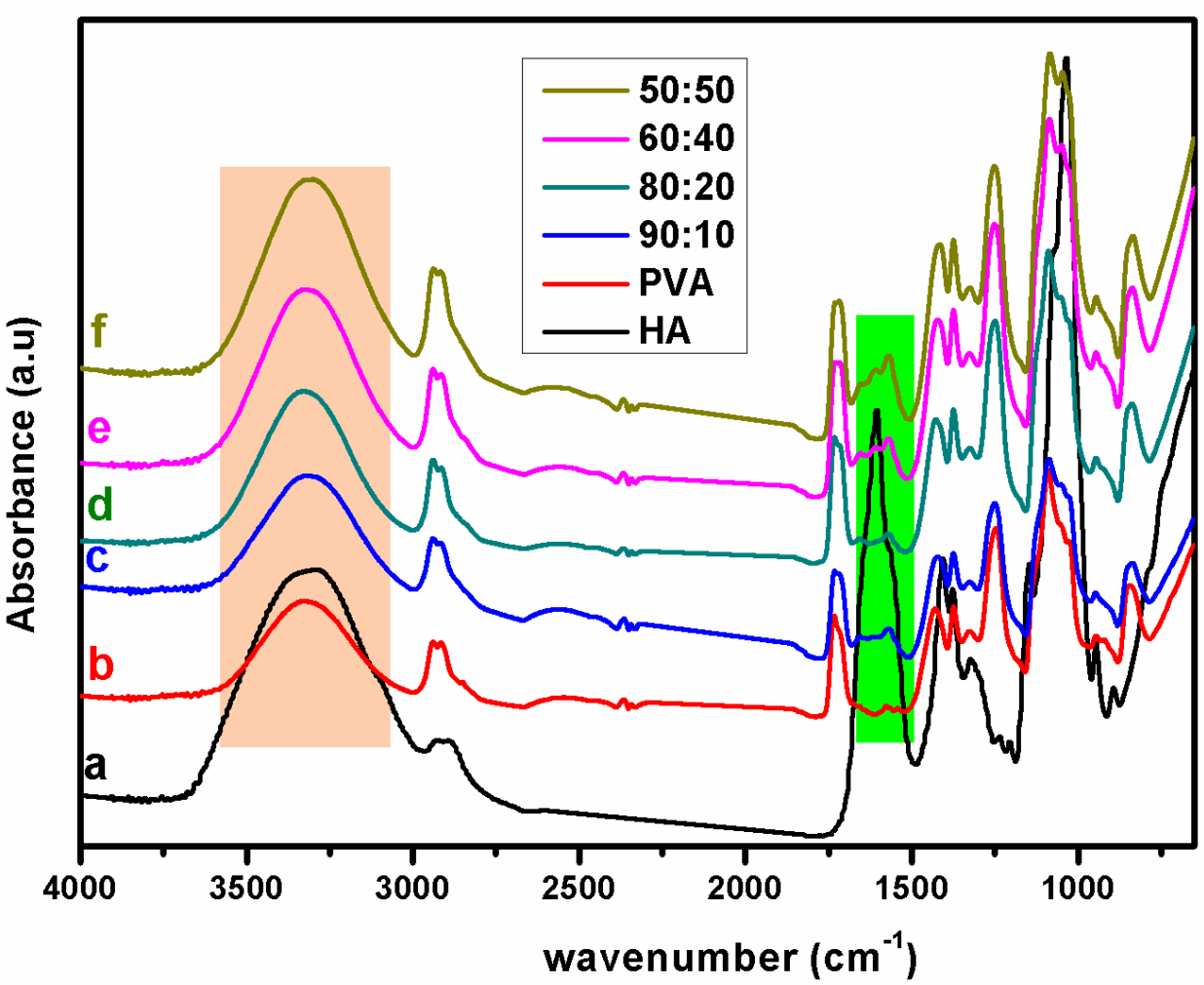


**Fig. 27:** FTIR spectrum of nanofiber sheet made of different ratios of HA/Ag-NPs and PVA

Note: experimental conditions: 2 % HA, 0.1 M $Ag^{+}$, 1 ml NaOH, 20 min, a) HA powder; b) PVA; c) ratio 90:10; d) ratio 80:20; e) ratio 60:40; f) ratio 50:50.

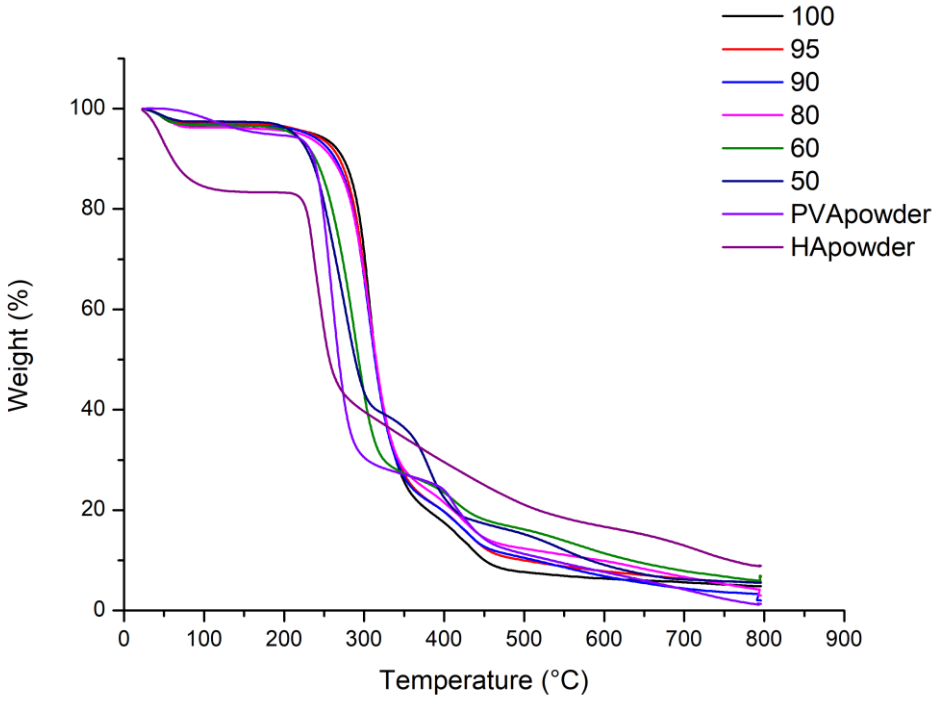


**Fig. 28:** TGA curves of 1 % HA/Ag-NPs : PVA nanocomposite and HA powder, PVA powder
Note: legend provides percentage content of PVA used for nanocomposite preparation; heating program: 10°C/min to 800° C under nitrogen atmosphere.

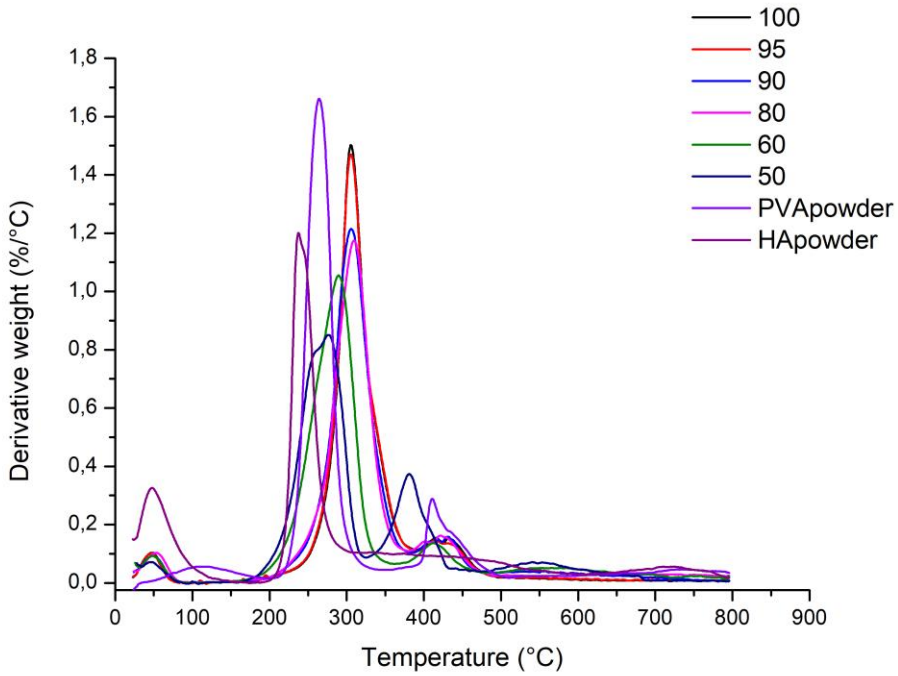


**Fig. 29:** DTG curves of 1 % HA/Ag-NPs : PVA nanocomposite and HA powder, PVA powder
Note: legend provides percentage content of PVA used for nanocomposite preparation; heating program: 10°C/min to 800°C under nitrogen atmosphere.

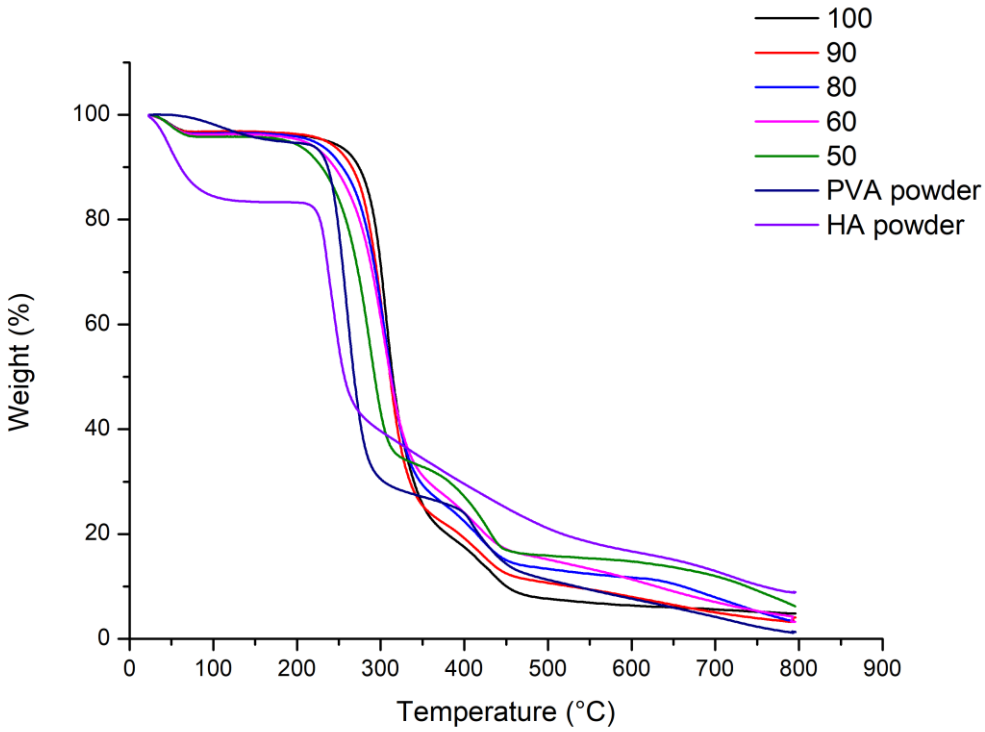


**Fig. 30:** TGA curves of 2 % HA/Ag-NPs : PVA nanocomposite and HA powder, PVA powder
Note: legend provides percentage content of PVA used for nanocomposite preparation; heating program: 10°C/min to 800°C under nitrogen atmosphere.

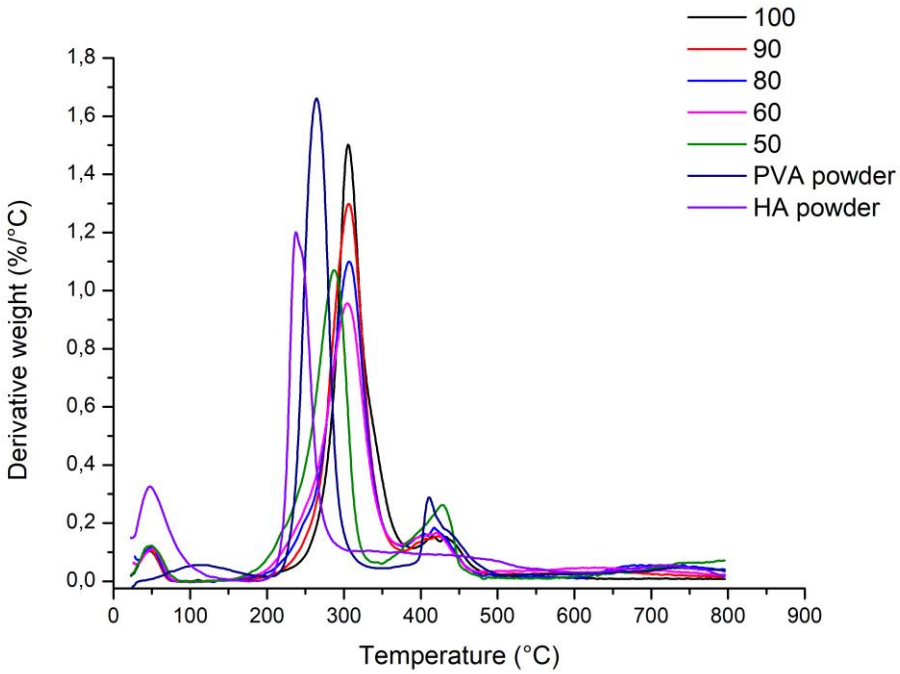


**Fig. 31:** DTG curves of 2 % HA/Ag-NPs : PVA nanocomposite and HA powder, PVA powder
Note: legend provides percentage content of PVA used for nanocomposite preparation; heating program: 10°C/min to 800°C under nitrogen atmosphere.

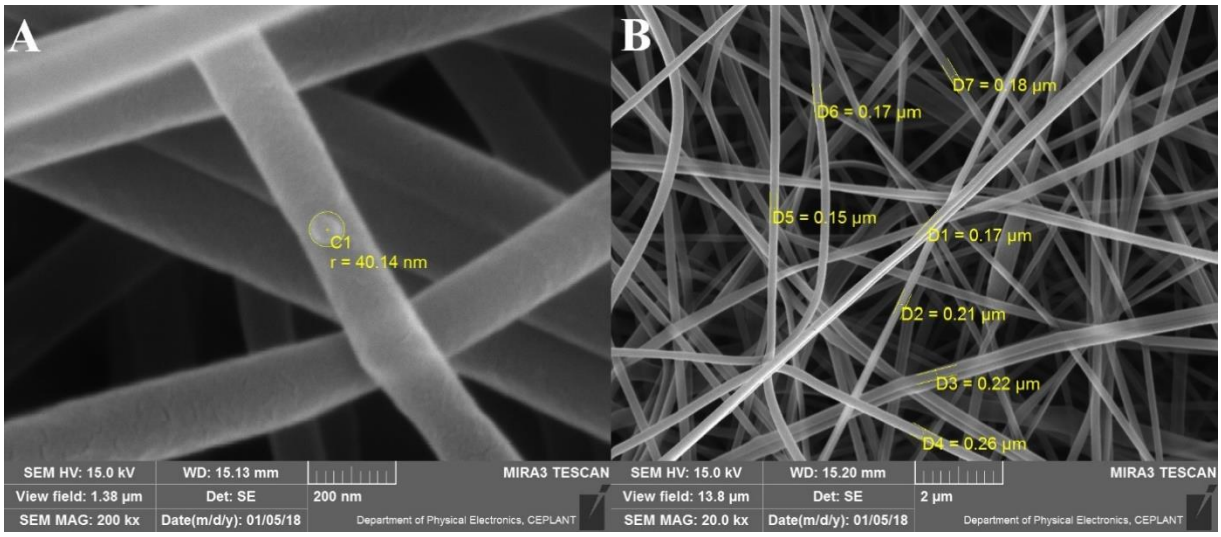


**Fig. 32:** SEM images of nanofibers with samples made of 1 % HA, A) Ag nanoparticle found at sheet with the ratio 10:90; B) ratio 5:95 with schematic illustration of measurement of the diameter of nanofibers by SEM software.